crystals

MDPI

Review

Review on Eutectic-Type Alloys Solidified under Static Magnetic Field

Hao Cai †, Wenhao Lin †, Meilong Feng, Tianxiang Zheng *, Bangfei Zhou * and Yunbo Zhong *

State Key Laboratory of Advanced Special Steel & Shanghai Key Laboratory of Advanced Ferrometallurgy & School of Materials Science and Engineering, Shanghai University, Shanghai 200444, China; caihao@shu.edu.cn (H.C.); wenhaol@shu.edu.cn (W.L.); fml2010@shu.edu.cn (M.F.)

* Correspondence: ztx@shu.edu.cn (T.Z.); zhoubf@shu.edu.cn (B.Z.); yunboz@shu.edu.cn (Y.Z.)

† These authors contributed equally to this work.

Abstract: Processing metallic alloys under a static magnetic field (SMF) has garnered significant attention over the past few decades. SMFs can influence both the thermodynamics and kinetics of the solidification process by introducing extra force and energy. Eutectic-type alloys (ETAs) are commonly used as research materials under SMFs due to their featured microstructures. This review aims to present theoretical and experimental results regarding ETAs under SMFs, from post-analysis to in situ observation, to demonstrate the effects of magnetic phenomena such as magnetic braking, thermoelectric magnetic convection, magnetic gradient force, and magnetic energy on the thermodynamics and kinetics of microstructural evolution. In this paper, we adopt a hybrid approach between a review and an overview to comprehensively examine the effect of SMFs on the solidification process. Firstly, we provided a concise review of the historical research on the SMF's impact on solidification in the literature. Next, we elucidated the basic physical principles of an SMF in material processing, followed by an introduction of numerous laboratory and industrial experiments that have utilized SMFs. Finally, we summarized the effects of SMFs on solidification in the past and provide insights into future research directions.

Keywords: static magnetic field; eutectic-type alloys; solidification; review

Citation: Cai, H.; Lin, W.; Feng, M.; Zheng, T.; Zhou, B.; Zhong, Y. Review on Eutectic-Type Alloys Solidified under Static Magnetic Field. *Crystals* **2023**, *13*, 891. https://doi.org/10.3390/cryst13060891

Academic Editor: Hongbin Bei

Received: 23 April 2023
Revised: 11 May 2023
Accepted: 16 May 2023
Published: 29 May 2023

1. Introduction

The solidification of ETAs has been widely studied and modeled for binary and most key ternary alloy systems. The development of eutectic microstructures in ternary, multi-component, and eutectic high entropy alloys (EHEAs) has led to the emergence of potential engineering materials exhibiting superior mechanical and magnetic properties compared to traditional binary eutectic alloys, owing to their refined microstructures and/or the presence of dual hard/soft phase mixtures [1]. The process of solidification plays a crucial role in determining the microstructural evolution of ETAs and achieving the desired physical or chemical properties. However, with the rapid advancement of science and technology, conventional solidification methods have proven insufficient in meeting the high-performance requirements of ETAs. As a result, additive manufacturing [2,3] and physical fields such as electric current [4], super/microgravity [5], ultrasonic fields [6], and magnetic fields [7,8] have been widely employed to modify the microstructures of metallic materials. Among these methods, SMFs, generated by permanent magnets, electromagnets, and superconductive magnets, have proven to be particularly effective and are now extensively used in advanced materials processing. Various intriguing experimental phenomena have been observed, including magnetohydrodynamics [9,10], magnetic levitation [11], magnetic orientation [12], and magnetic thermodynamic effects [13]. These well-known contactless forces and energy effects deepen our understanding of controlling the solidified microstructure using SMF and offer promising applications in the industrial area.

To investigate the effect of a high SMF on the solidification process of ETAs, various master alloys, such as Al-Cu [14–17], Nb-Fe [18], Cu-Ag [19,20], Al-Si [21–23], Al-Mg [24], Al-Fe [25–28], Al-Ni [29], Al-Zn [30], Sn-Bi [31–33], Pb-Sn [34–36], Zn-Mg [37,38], Mg-Nd [39], Co-B [40,41], Co-Sn [42], Mn-Sb [43], Bi-Mn [44], Al-Si-Fe [45], Al-Cu-Ag [46], Al-Cu-Si [47], and NiAl-Cr(Mo)-Hf [48] have been selected for investigation and the research contents are listed in Table 1. During the investigation of solidification of ETAs under the SMF, the solidification theories under the SMF were gradually established. Researchers explored the use of the well-known magnetic braking effect caused by the magnetic braking force to reduce segregation in the melt by eliminating thermal convection [49]. A new thermoelectric magnetic (TEM) convection was discovered to be useful in tailoring the microstructure [31,50]. This convection is induced by a Lorentz force called TEM force, created by the interaction between the thermoelectric current near the solid–liquid interface and the applied SMF [19]. The TEM force, which has been extensively investigated over the past two decades, provides an effective method to control melt convection and the morphology of the solid–liquid interface in the mushy zone. Additionally, the magnetic gradient force has been used to control solute or particle migration during solidification under the gradient SMF [7]. Recently, magnetic dipole–dipole interactions (or magnetic interaction force) have been successfully used to affect grain growth, resulting in elongated grain and chainlike microstructures [40], and control the agglomeration and dispersion of primary crystals [51]. Therefore, the aforementioned forces, which have significant effects on the kinetic processes of solidification, are effective in controlling atom diffusion [52–56], nucleation events [42,57], melt convection [19,34], solute distribution [32,58,59], crystal migration [21,43,60], and morphology evolution [61–63] during solidification. Apart from kinetic processes, magnetic energy can also modify thermodynamic events, such as phase transformation and crystal orientation, even in a non-ferromagnetic system [12,64,65]. Indeed, the crystal orientation is considered to be influenced by the SMF in both thermodynamic and kinetic ways. In the past decade, our group has systematically investigated the role of SMFs in the solidification process, including atomic diffusion [55,56,66,67], dendrite growth [61,68], homogenization of the secondary phase in immiscible alloy [69–71], and electroslag remelting in steel [72–74]. Based on these studies, we suggested that ETA materials processing under an SMF holds promise for both fundamental scientific research and industrial applications.

Table 1. Summary of ETAs investigated under SMFs.

ETAs	*B* (T)	Research Content	References
Al-Cu	0–10	Eutectic spacing; microstructure evolution, orientation of Al_2Cu; interface shape	[14–17]
Nb-Fe	1–5	Phase separation	[18]
Cu-Ag	0–200 mT, 0–31.2	TEM convection in the melt; microstructure, electrical resistivity, magnetoresistance	[19,20]
Al-Si	0–12	Distribution of primary silicon under uniform and gradient magnetic field; arm spacing, eutectic lamellar spacing; refinement of primary silicon	[21–23]
Al-Mg	0, 8.8	Solute segregation	[24]
Al-Fe	0–12	Distribution of primary phase	[25–28]
Al-Ni	0–2	Microstructural evolution	[29]
Al-Zn	0, 5	Dendrite morphology and growth orientation	[30]
Sn-Bi	0–0.55	TEM convection in the melt; microstructural evolution and solute distribution; refinement of arm spacing	[31–33]

Table 1. *Cont.*

ETAs	*B* (T)	Research Content	References
Pb-Sn	0–12	Convection and macrosegregation; TEM convection and microstructural evolution; dendrite morphology	[34–36]
Zn-Mg	0–12	Orientation of primary Zn-rich crystals; the morphology, size, and distribution of the primary $MgZn_2$ crystals	[37,38]
Mg-Nd	0, 1	Phase formation	[39]
Co-B	0–4T	Morphology and magnetic alignment of the primary α-Co phase	[40,41]
Co-Sn	0–12	Nucleation behavior	[42]
Mn-Sb	0–11.5	Orientation of both the primary and eutectic MnSb crystals	[43]
Bi-Mn	0–10	Growth of eutectic Bi/MnBi	[44]
Al-Si-Fe	0, 0.07	Precipitation behavior of iron intermetallic compounds	[45]
Al-Cu-Ag	0–6	Microstructural evolution	[46]
Al-Cu-Si	0–0.5	Evolution of microstructure and crystallization	[47]
NiAl-Cr(Mo)-Hf	0–6	Microstructural evolution	[48]

In this review, we summarize the progress in processing ETAs under the SMF conditions. Based on the fundamental physical principles that govern the effect of magnetic fields on the solidification of ETAs, this paper provides a comprehensive review of the impact of SMFs on microstructure thermodynamics and kinetics under various solidification conditions. Through a detailed analysis of relevant experiments, this review offers valuable insights for researchers to choose appropriate SMF modes and solidification conditions to achieve desirable microstructures and corresponding material properties.

2. Basic Physical Principles and General Experimental Methods of SMFs in Material Processing

The influence of an SMF on the solidification process can be attributed to two main mechanisms: force and energy. During solidification, two types of magnetic forces can act on the melt and/or solid. The first type is the Lorentz force, arising from the coupling of an electric current and the SMF. This force is often utilized to control melt convection during solidification. The electric current can be induced by an external electric field, a conductive fluid across the field lines, or a thermoelectric current. In this study, we focus primarily on the induced current during solidification. The second type of magnetic force is the magnetization force, which arises from the physical properties of materials under a gradient SMF. This force is employed to control crystal migration or levitate diamagnetic materials. In addition to the force effects, magnetic energy cannot be ignored, especially in a high SMF, as it can influence the thermodynamics of the liquid-to-solid transformation and crystal orientation.

2.1. Magnetic Force

When a conductive flow is moving across the field lines, a Lorentz force is then induced by the coupling between the induced electric current and SMF to damp the melt flows. This Lorentz force can be expressed as follows:

$$\boldsymbol{F} = \boldsymbol{J} \times \boldsymbol{B} = \sigma(\boldsymbol{u} \times \boldsymbol{B})\boldsymbol{B} \quad (1)$$

where $\boldsymbol{J}$ is the electric current density, $\boldsymbol{B}$ is the magnetic flux density (MFD), σ is the electric conductivity of liquid, and $\boldsymbol{u}$ is the velocity of flow.

However, when a temperature gradient exists at the solid–liquid interface, a thermoelectric current then will be induced due to the Seebeck effect. Then, a new force called the TEM force is produced by the interaction between the thermoelectric current in the vicinity

of the solid–liquid interface and the external SMF. The TEM force can be simply shown as the following [75]:

$$\boldsymbol{F_{TEM}} = \boldsymbol{J_{TE}} \times \boldsymbol{B} = \frac{\sigma_s \sigma_l f_s}{\sigma_s f_s + \sigma_l f_l}(S_l - S_s)\nabla \boldsymbol{T} \times \boldsymbol{B} \tag{2}$$

where $\boldsymbol{J_{TE}}$ is the thermoelectric current, σ_s and σ_l are the electric conductivities of solid and liquid, respectively, f_s and f_l are the solid and liquid fractions, respectively, S_s and S_l are the thermoelectric powers of solid and liquid, respectively, and $\nabla \boldsymbol{T}$ is the temperature gradient. This TEM force can act both on the liquid and the solid, which triggers different phenomena.

Another Lorentz force comes from the differences of electric conductivity between the primary particle/inclusion and liquid. The total forces that act on a particle can be expressed as follows [76]:

$$\boldsymbol{F_P} = -V_P \frac{3}{2} \frac{\sigma_l - \sigma_P}{2\sigma_l + \sigma_P} \boldsymbol{J} \times \boldsymbol{B} \tag{3}$$

where V_P is the volume of the particles, and σ_P is the electric conductivity of the particle. Then, the moving direction of the particle is dependent on the magnitude of electric conductivity between liquid and particle.

In an inhomogeneous and a gradient SMF, a magnetic force is exerted on the material. This force can be expressed as follows [49]:

$$\boldsymbol{F_m} = V_P \frac{\chi_P}{\mu_0} \boldsymbol{B} \nabla \boldsymbol{B} \tag{4}$$

where, χ_P is the magnetic susceptibility of the particle or primary crystal, χ_P is the magnetic susceptibility of liquid metal, and μ_0 is the magnetic permeability of vacuum. By using a high SMF (greater than 15 T), materials such as Bi, Sb, wood, and water can be stably levitated when the magnetic force is equal and opposite to the gravitational force [77].

2.2. Magnetic Energy

The phase transformation process is primarily governed by thermodynamics. Temperature and pressure are well-known thermodynamic parameters that determine the energy of a system, but the SMF is also an important factor that should not be overlooked. Despite the fact that the magnetic energy of a substance at room temperature is much smaller than its thermal energy, the effect of SMFs on the phase transformation process has received little attention until recently. With the rapid development of high SMF generation technology, it is now possible to generate SMFs up to 45 T in the laboratory. When an SMF is applied to a system, the change in Gibbs free energy can be expressed as follows [4]:

$$\mathrm{d}G = -S\,\mathrm{d}T + V\,\mathrm{d}p - M\,\mathrm{d}B + \sum_i \mu_i\,\mathrm{d}n_i \tag{5}$$

where S is the entropy, T is the temperature, V is the volume, M is the magnetization, and μ_i is the chemical potential of component i. Thus, the total magnetic free energy in the system with an applying SMF can be derived as

$$G_m = -\int_0^B M\mathrm{d}B = -\int_0^B \frac{V\chi}{\mu_0} B\,\mathrm{d}B \tag{6}$$

The magnetic energy can not only influence the temperature of phase transformation [13,65,78] but also the orientation of materials [30,64], which will be shown in the following section.

2.3. General Experimental Methods

In this part, we first introduce the magnet to produce an SMF, and then the experiment's machines used to study the solidification process under the SMF are also briefly introduced.

2.3.1. Magnetic Field Generator

Various types of SMFs can be generated depending on the application, from weak fields of less than 1 T to high SMFs of tens of tesla. Permanent NdFeB magnets (Figure 1a) are typically used to produce weak SMFs during in situ observation experiments [79]. Electromagnets (Figure 1b) can produce fields up to approximately 1 T and are commonly used in material processing due to their convenience. To produce high SMFs of around 10 T, superconducting magnets (Figure 1c) are used and are available in the laboratory. Bitter magnets (Figure 1d) can generate SMFs greater than 20 T and are now accessible in several countries, such as China, France, Japan, the Netherlands, and USA.

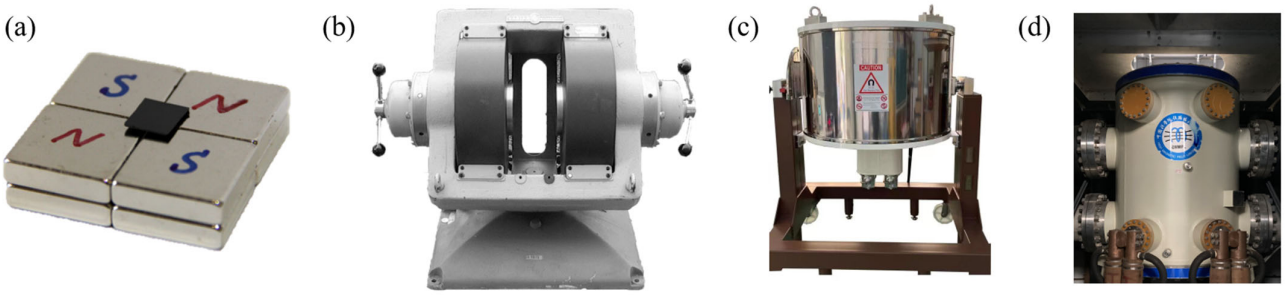

Figure 1. (**a**) NdFeB permanent magnet, the black material is a piece of graphene [79]. (**b**) Electromagnet (Varian V3703, Palo Alto, CA, USA). (**c**) Superconducting magnet (JMTD-10T180MK II, JASTEC, Tokyo, Japan). (**d**) Bitter magnet (25 T-50 mm bore, High Magnetic Field Laboratory of Chinese Academy of Science, Hefei, China).

2.3.2. General Experimental Facilities

Directional solidification is the preferred method for studying crystal growth under SMFs, as it allows for control of temperature gradient, heat flow direction, and growth velocity at the solid–liquid interface. Figure 2a shows a schematic diagram of the directional furnace (also known as the Bridgman furnace) under the SMF [30]. By quenching the sample into the Ga-In-Sn cooling medium, the solid–liquid interface and mush zone can be obtained under the SMF, allowing for key information such as morphology, dendrite spacing, and solute distribution to be acquired. The solidification process can then be conducted in the homogeneous or gradient region of the magnetic field by adjusting the sample's location.

Isothermal solidification without or with a very weak temperature gradient during solidification is another essential solidification method. Figure 2b shows a copper furnace with a 70 mm isothermal zone designed for solidification under a high SMF (>20 T) [80]. The ex situ observation procedure of materials is also shown in Figure 2b, where the distribution and morphology of the microstructure can be obtained in a three-dimensional manner assisted by X-ray computed tomography (XCT). In situ observation of solidification under permanent magnet or electromagnets can now be achieved by synchrotron radiation. As shown in Figure 2c, an electromagnet which can generate a magnetic field of 1 T between two iron cores can be used for in situ observation process. The SMF can act on the solid–liquid interface to control the microstructure during directional solidification [81]. Encapsulation of the sample is crucial for in situ observation of the solidification process as illustrated in Figure 2d.

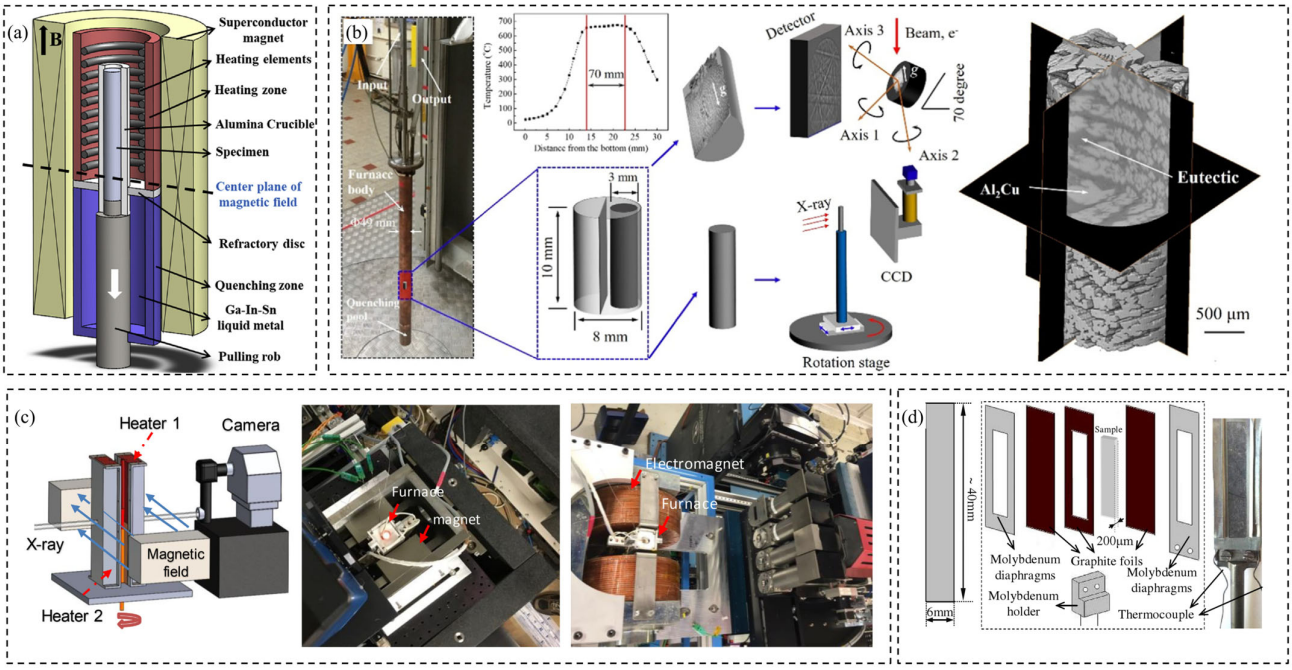

Figure 2. General experimental devices for solidification under the SMF. (**a**) Schematic diagram of device for Bridgman directional solidification [30]. (**b**) Isothermal solidification furnace designed for high SMFs and the ex situ observation of material by X-ray computed tomography technique [80]. (**c**) In situ observation devices of solidification under SMF [81]. (**d**) Sample encapsulation method for in situ observation [82].

3. Magnetohydrodynamic Effect

3.1. Magnetic Braking Effect during Solidification

The magnetic braking effect is based on the use of the Lorentz force, which arises from the interaction between the electric current density ***J*** and the magnetic flux density ***B*** in the melt. The solidification microstructure of ETAs is difficult to control due to the complex interplay between temperature, solute, and melt. In terrestrial experiments, convections generated by density and temperature differences, as well as Marangoni effects caused by surface temperature gradients, may result in solute segregation during solidification and damage the material's properties. In fact, the unavoidable convection on the ground, which leads to the instability of crystal growth, segregation, and local freckles, interferes with our understanding of the solidification process.

It is well known that the SMF, which was used to improve the quality of cast products of steel [83], can damp the movement of conductive melt. Another important application of the magnetic braking effect is in the growth of semiconductor crystals. Researchers [49] found that the SMF could eliminate the solute segregation in the growth process of semiconductor single crystals by eliminating thermal convection in the melt. Subsequently, the braking effect of SMFs on solidification was widely studied, ranging from pure metals to alloys [9,10] and from experiments to numerical simulations [84–87]. Although these studies have deepened our understanding of the braking effect, the weak MFD still limits our ability to provide a pure diffusive growth condition suitable for the steady growth of metallic crystals.

Studies have shown that the diffusion coefficient value decreases with the increase in MFD, which provides a simulated diffusive condition [52–54]. Recently, a novel gravity-assisted automatic docking (GAAD) device was independently developed to measure the interdiffusion coefficient of an Al-Cu alloy (D_{AlCu}) from 0 T to 22 T and the critical MFD for achieving the diffusion-limited condition [55,56], as shown in Figure 3a–c. The details of the GAAD apparatus can be found in Refs. [55,56]. Results demonstrated that the diffusion-limited condition as measured in microgravity was achieved when the MFD was greater

than about 3 T. To further reveal the influence of this diffusive condition on crystal growth, Al-20wt.%Cu hypoeutectic alloy was solidified under a 24 T high SMF (Figure 3d–f) [61]. In this diffusive condition, the primary dendrite maintained stable growth and side arms with small surface curvatures that grew nearly perpendicular to their stem. Additionally, the secondary dendrite arm spacing (SDAS) increased. This is consistent with results under microgravity [88]. The braking effect was also used to obtain a directional microstructure using a solute gradient rather than a temperature gradient [89,90]. As Asai pointed out [91], the magnetic braking effect was a useful way to understand crystal growth. However, there is still a lack of research on the effect of the diffusive condition created by high SMF on the dynamics of metallic crystal growth, including growth velocity, morphology, surface evolution of crystals, and diffusion in the solute boundary layer. Compared with high cost and limited experiment time in space or space shuttles, simulated diffusive conditions created by high SMFs is a promising way to study the growth of crystals. However, these aspects require further study.

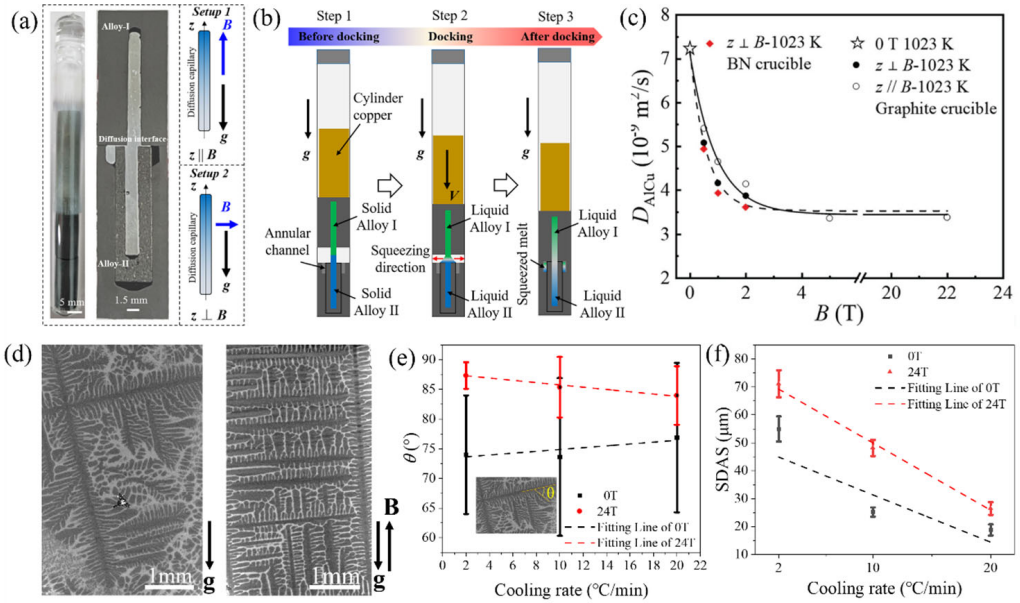

Figure 3. (**a**) Diffusion couple and schematic diagram of setups under SMF. (**b**) Schematic diagram of the GAAD. *V* is the direction of movement of copper cylinder. Alloy I and II are Al-25at.%Cu and Al-15at.%Cu, respectively [56]. (**c**) The relationship between the D_{AlCu} and the MFD. The solid fitted line corresponds to setup 1 at 1023 K, the dashed fitted line to setup 2 at 1023 K. (**d**) Microstructures of Al-20wt.%Cu alloys solidified without and with a 24 T high SMF, respectively. (**e**) Angles between the side arms and stems without and with 24 T high SMF, respectively. (**f**) The SDAS versus cooling rate without and with 24 T high SMF, respectively [61].

3.2. TEM Effect during Solidification

By observing the fluidity of liquid metal under the SMF, Shercliff first proposed the theory of TEM convection in 1979 [50]. Later, Alboussiere [75] gave an expression of thermal current through the theoretical analysis of interdendritic flow under the SMF. Figure 4a shows that the thermoelectric current works in two mediums with different thermoelectric powers. During solidification, three conditions should be satisfied to create the thermoelectric current [92]:

(1) The thermoelectric powers of the liquid and the solid must be different, $S_l - S_s \neq 0$.
(2) A temperature gradient exists at the vicinity of the interface.
(3) The temperature gradient must not be perpendicular to the interface.

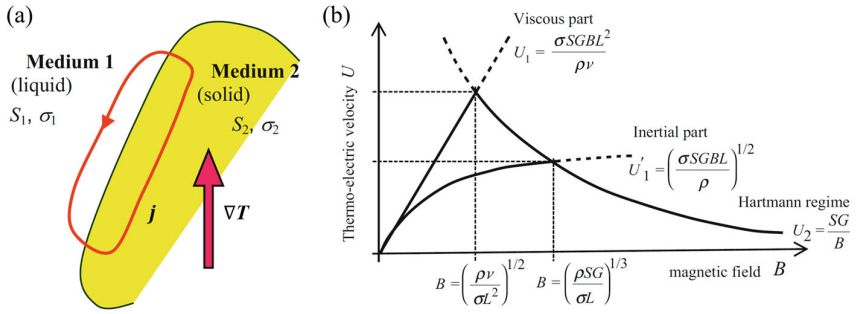

Figure 4. (**a**) A sketch of the thermoelectric current distribution near the interface between two media. (**b**) A schematic illustration of the evolution of TEM velocity, U as a function of MFD, B [83]. S is the thermoelectric power, L is the typical length, G is the temperature gradient, ρ is the density.

The velocity of TEM convection can be estimated from the data from Ref. [93], which is shown in Figure 4b. In a certain temperature gradient and a typical length of the system, the TEM convection first increases then decays with the increase in MFD.

In recent decades, researchers have extensively studied the TEM convection caused by TEM forces during directional solidification. At the beginning of the 21st century, Li and his colleagues [16,62,94–96] conducted a series of directional solidification experiments under SMFs and systematically studied the influence of TEM forces and convection on solidification microstructures. Their work significantly advanced our understanding of microstructure control under SMFs. Although the TEM force and convection phenomena were observed from the post-analysis of the solidified samples in the early 21st century, direct observation evidence was lacking until Yasuda's in situ solidification experiment of Al-Cu alloys under an SMF in 2012 [97]. Wang et al. [82,98] then directly observed dendrite fragmentation and the transition of the inclined solid–liquid interface from convex to flat after the application of an SMF (0.08 T) by using synchrotron radiation and further confirmed the existence of TEM force and convection. This new convection offers possibilities to design materials with different microstructures using SMFs.

Solute segregation during solidification can have negative impacts on the final microstructure and properties of materials. One of the challenges in solidification science is to achieve solute homogenization in the ingot, which can be accomplished through methods such as stirring or vibration. A promising technique for eliminating solute segregation bands is the application of SMFs. Researchers [49] demonstrated that the magnetic braking effect of the SMF could eliminate solute segregation bands caused by turbulent thermal convection during the solidification process. However, when solidification occurs under a weak SMF (<1 T), the interdendrite channel size is too small to induce a magnetic braking effect, and the change in microstructure is attributed to the TEM convection [19].

The thermoelectric power of common eutectic metallic alloys is generally weak, with an order of magnitude of 10^{-6} V/K. Therefore, according to Equation (2), the TEM force is proportional to the magnitude of the MFD. At a high SMF of 10 T, the TEM force is comparable to gravity and can act on the liquid melt to induce TEM convection as well as on solid to break dendritic arms [96]. It is well known that a transverse SMF can induce unidirectional flow in the melt at the solid–liquid interface, leading to an inclined solid–liquid interface, which can trigger solute segregation channels or side segregation in the ingot [16,92,99]. For an axial SMF, an annular flow pattern of TEM convection was generated, resulting in an azimuthal channel flow in the interdendrite area [16]. This flow pattern was useful for controlling the morphology of the solid–liquid interface and refining the microstructure [16,100]. The strength of the TEM convection depends on temperature gradient, chemical composition, and MFD, which can be adjusted to control the TEM force and convection.

Recent research has focused on the distribution of solutes under high SMFs during solidification and semi-solid heat treatment [59,101,102]. For example, the application of

a high SMF changed the solute interception among dendritic arms in the mushy zone of a Mn-Sb alloy, resulting in the precipitation of Sb-rich phases in the matrix [101]. In an Al-Cu alloy, an increase in MFD resulted in a decrease in the fraction of non-equilibrium eutectic and an increase in Cu solute in the primary phase [58]. Authors suggested that the TEM convection in the melt accelerated solute diffusion, and TEM force in solid promoted more dislocations to entrap solute. He et al. [59] also found that a high SMF increased the effective partition coefficient of Al-4.5wt.%Cu and inhibited diffusion behavior in the solid.

High SMFs have been proven to destabilize cellular and dendritic morphology, as discussed in previous work [62]. The destabilization of dendrites and occurrence of columnar-to-equiaxed transition (CET) during directional solidification of Al-Cu, Pb-Sn, and Al-Si alloys were attributed to the TEM force acting on the solid, as well as changes in surface chemical potential and surface tension [103]. In contrast, the moderate SMF was observed to form ring-like structures in the mush zone of hypoeutectic alloys due to TEM convection in the interdendritic area. However, the appearance of these structures was found to disappear upon increasing the SMF, which was attributed to the braking effect at high SMF, as shown in Figure 5a. In the case of Al-Al_2Cu eutectic alloys, a high SMF was found to decrease eutectic spacing, degenerate the lamellar structure, and trigger band-like segregation at low growth speeds, as shown in Figure 5b [14]. Similarly, a high SMF in Al-Al_3Ni fiber eutectic alloys decreased the eutectic spacing and caused land-like structures, as well as altered the orientation relationship between Al and Al_3Ni [104]. The effect of a high SMF on ternary eutectic alloys was first investigated in Al-Cu-Ag alloys, with results indicating modifications to the microstructure and orientation relationship between eutectics at lower growth speeds under high SMFs (up to 6 T). Additionally, SMFs reduced eutectic spacing and caused the formation of banded structures at lower growth speeds ($R < 0.8$ μm/s). Authors suggested that the TEM effect altered the interfacial energy and led to modifications in the solidification microstructure and orientation relationship [46]. In hypereutectic alloys, the effect of an SMF was similar to that observed in hypoeutectic alloys, as shown in Figure 5c [105]. Transverse SMFs triggered inclined solid–liquid interfaces and accelerated segregation, but an external electric current was applied to the sample to induce an electromagnetic (EM) convection, which counteracted the TEM convection and weakened the destruction of solidification microstructure caused by the TEM effect (Figure 5(d1–d3)). When the EM convection was equal to the TEM convection, the interface was nearly flat, while the inclined interface changed to the other side when the EM convection was greater than the TEM convection [99].

Although many works have been performed on the post-analysis of optical and SEM images of solidified ingots treated with SMFs, in situ observations of the dynamic solidification process are still lacking. Direct observation of TEM convection was first conducted by Yasuda et al. [97] in unidirectionally solidified Al-15wt.%Cu alloys (size: $10 \times 10 \times 0.1$ mm^3) at the Spring-8 synchrotron radiation facility under 0.45 T, as depicted in Figure 6a,b. The observed transverse movement of fragments was attributed to the TEM convection. In a similar experiment, Wang et al. [82] observed the movement of fragments in situ in Al-4wt.%Cu at the European Synchrotron Radiation Facility under a 0.08 T SMF and established a model to calculate the velocity of particles, as shown in Figure 6c–g. Although they supposed that the TEM force promotes fragmentation, Fautrelle et al. [92] suggested that this moderate SMF may be insufficient to bend dendrite arms. To further prove the existence of TEM convection during solidification, Wang et al. [98] conducted in situ observations of the planar solid–liquid interface under SMFs, which showed that the inclined interface was modified into a planar one. They suggested that TEM convection resulted in the experimental phenomena shown in Figure 6h–n. Additionally, solidification of a Ga-In alloy was observed in situ under a 0.19 T SMF using an X-ray imaging facility in the laboratory [106]. By linking the evolution of microstructures under SMFs with time, researchers can propose models to predict microstructural evolution.

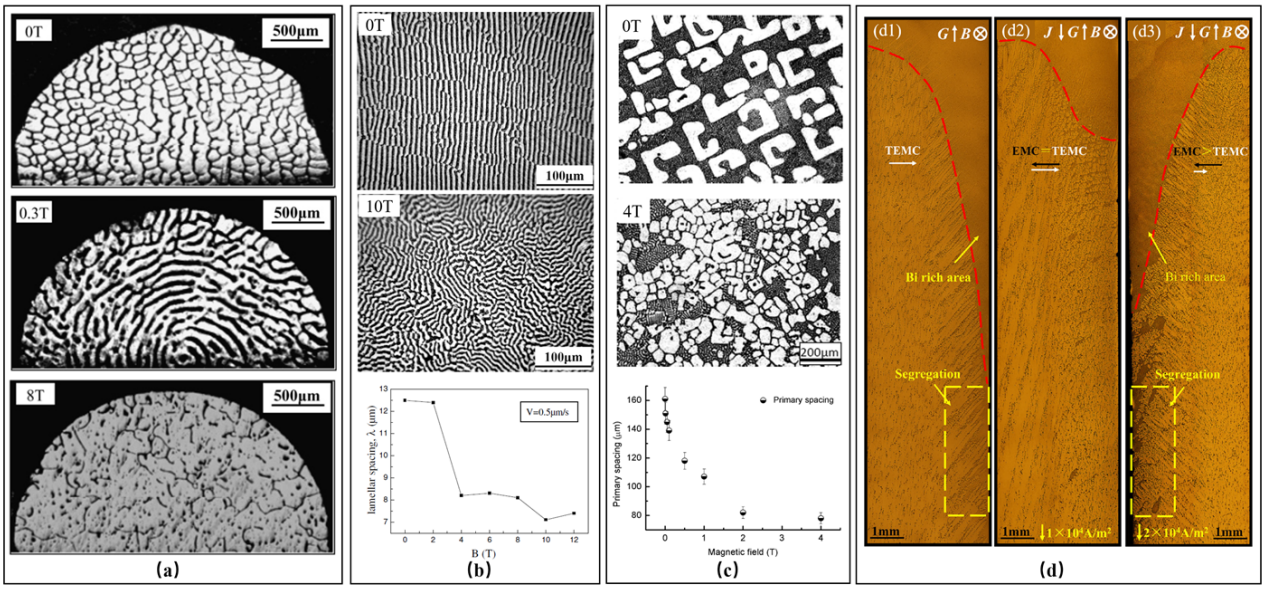

Figure 5. (**a**) Transverse structures in the mushy zone in Al-0.85wt.%Cu alloys under SMF (G = 62.8 K/cm and pulling rate was 10 μm/s) [16]. (**b**) Eutectic microstructure solidified without and with 10 T SMF, and the lamellar spacing varies with MFD (G = 66.8 K/cm and pulling rate was 1 μm/s) [14]. (**c**) Morphology of primary Al_2Cu phase in directionally solidified Al-40wt.%Cu alloy in various MFDs (G = 62 K/cm and pulling rate was 2 μm/s) [105]. (**d**) Directionally solidified microstructures of Sn-10wt.%Bi alloys at 10 μm/s under a 0.5 T transverse SMF with and without the external direct current [99] (TEMC = TEM Convection, EMC = Electromagnetic Convection, J represents the external direct current).

Engineering materials are typically composed of polycrystals, making it crucial to understand the spatial effects of SMFs on the solidification process. In the 3D imaging field, Koe et al. [107] developed a novel electromagnetic apparatus for in situ synchrotron X-ray imaging to study the separation of phases in metal solidification, showing brief results for Al-20wt.%Si. The first 4D (3D plus time) experiment under an SMF was conducted by Cai et al. in an Al-15wt.%Cu alloy under a 0.5 T SMF [81]. This study coupled high-speed synchrotron X-ray tomography and high-performance computational simulation to reveal the evolution, dynamics, and mechanisms of solidification, unraveling the complex interplay and competing flow effects arising from the Lorentz forces of different origins. Researchers obtained an Archimedes screw-like structure (Figure 7a) and a highly refined dendritic primary array. Through experiments and simulations, they also demonstrated that alloy composition could be tailored to increase or decrease the influence of magnetohydrodynamics depending on the Seebeck coefficient and relative densities of the primary phase and the interdendritic liquid melt. This study deepens our understanding of using Lorentz forces to design novel microstructures.

In another study, Song et al. [108] used in situ synchrotron XCT to report the faceted growth of Al_2Cu intermetallic compounds (IMCs) in Al-40wt.%Cu alloy directionally solidified under a 0.5 T SMF. They observed and studied the coarsening process of Al_2Cu IMCs in the overview of the 4D microstructure without and with the SMF (Figure 7b,c). The refinement effect disappeared when the temperature gradient was close to zero under SMF, indicating that TEM convection could be ignored in this case. By using 4D synchrotron XCT, Cao et al. [45] studied the influence of the transverse SMF (0.07 T) on the growth of iron IMCs during solidification of an Al-Si-Fe alloy. The results showed that TEM force had potential in removing Fe elements for recycling pure Al (Figure 7d,e). In situ observation experiments under SMF can help us to further understand the evolution and the dynamics of crystal growth of ETAs.

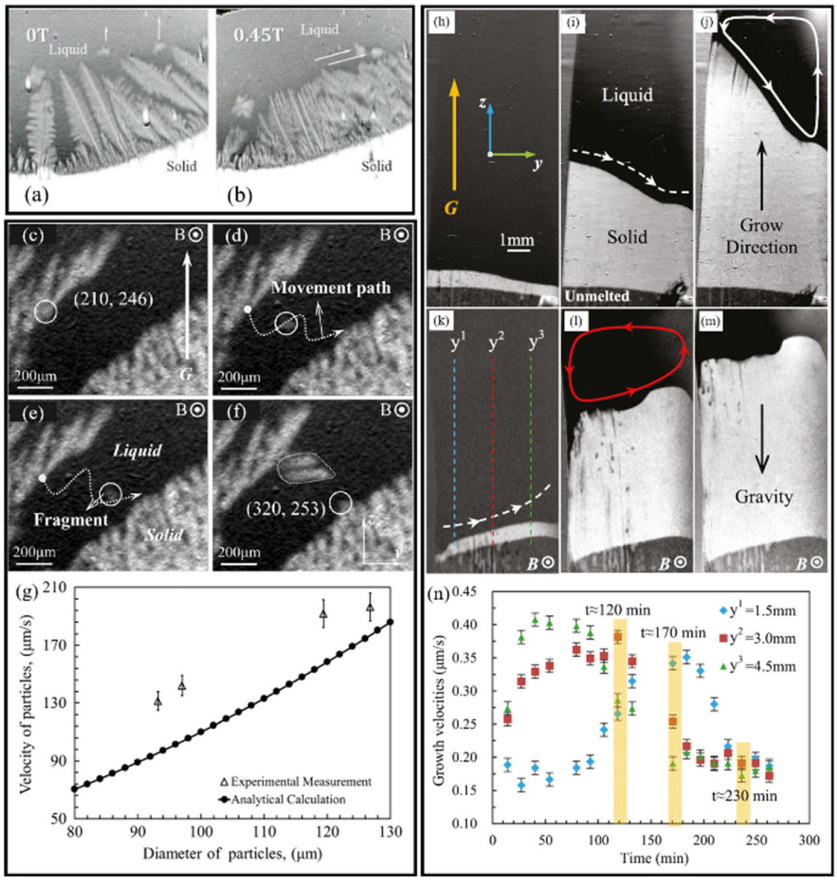

Figure 6. Directional solidification of Al-10wt.%Cu alloys (pulling rate = 10 μm/s, temperature gradient ≈ 3 K/mm). (**a**) 0 T; (**b**) 0.45 T [97]. Successive images of the motion of fragment in Al-4wt.%Cu alloy under a 0.08 T SMF during in situ synchrotron X-ray observation. (**c**) One frame before the fragment began to move, $t \approx 7077.0$ s; (**d**) $t \approx 7078.4$ s; (**e**) $t \approx 7079.8$ s; (**f**) $t \approx 7081.2$ s. (**g**) Analytical calculation and the experiment data of particle velocity versus its diameter [82]. Sequenced images of directional solidified Al-4wt.%Cu alloy (**h**–**j**) without and (**k**–**m**) with a 0.08 T transverse SMF, $B = 0.08$ T; (**h**) $t \approx 40$ min; (**i**) $t \approx 200$ min; (**j**) $t \approx 360$ min; (**k**) $t \approx 20$ min; (**l**) $t \approx 200$ min; (**m**) $t \approx 290$ min ($G = 3500$ K/m and cooling rate of 0.1 K/min). (**n**) Growth velocities of solid–liquid interface varies with time [98].

However, due to limitations of technique, in situ observation of the solidification process under the high SMF (>1 T) remains a challenge. Ex situ observation using XCT in the laboratory provides an alternative approach to investigate the 3D information of crystals under a high SMF. The 3D morphology of dendrites under directional solidification has been studied using XCT [30,80]. Lin et al. [61] reconstructed the 3D morphology of primary α-Al dendrites treated by a 24 T high SMF during bulk solidification and found that the dendrite growth was stable, and the dendrite size increased under the high SMF. Researchers suggested that this simulated microgravity environment achieved by high SMF has potential for tailoring single metallic crystals [68].

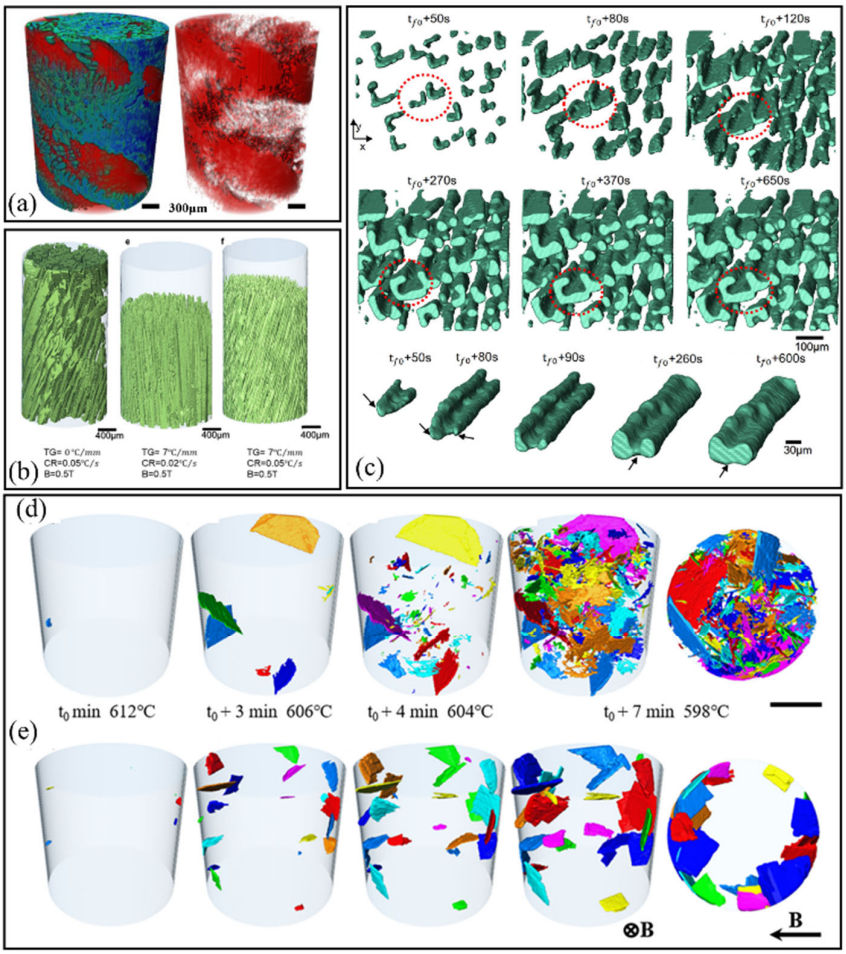

Figure 7. (**a**) The formation of screw microstructure in Al-15wt.%Cu under different thermal conditions in an SMF (G = 5 K/mm, cooling rate was 0.05 K/s and B = 0.5 T) [81]. (**b**) Overview of microstructures in 3D [108]. (**c**) Formation processes and faceted to non-faceted transition of Al_2Cu intermetallic compound clusters in Al-40wt.%Cu (cooling rate was 0.05 °C/s, G = 7 °C/mm and B = 0.5 T) [108]. (**d**,**e**) The evolution processes of IMCs during solidification of Al-10wt.%Si-1wt.%Fe alloy without and with SMF, respectively [45].

4. Magnetic Force during Solidification

The utilizing of a gradient SMF for the contactless magnetic separation of materials with different magnetic properties has gained significant attention in recent years. With advancements in magnet techniques, gradient high SMFs can be produced in the laboratory, achieving even the levitation of Bi and Sb metals when the gradient product BdB/dz approaches 1000 T^2/m [77]. This provides new opportunity for efficiently controlling the migrations of solutes and particles.

In particular, recent studies have focused on the use of a gradient high SMF to control the microstructure of ETAs during solidification, with the aim of solving solute segregation issues and designing new microstructures. Solidification of ETAs, including Al-Si [21], Al-Mg [24], Al-Fe [25,26,28], and Mn-Sb [8,60], has been performed under the gradient high SMF. These investigations demonstrated that both solutes and primary particles could be successfully controlled through the magnetic force, as shown in Figure 8.

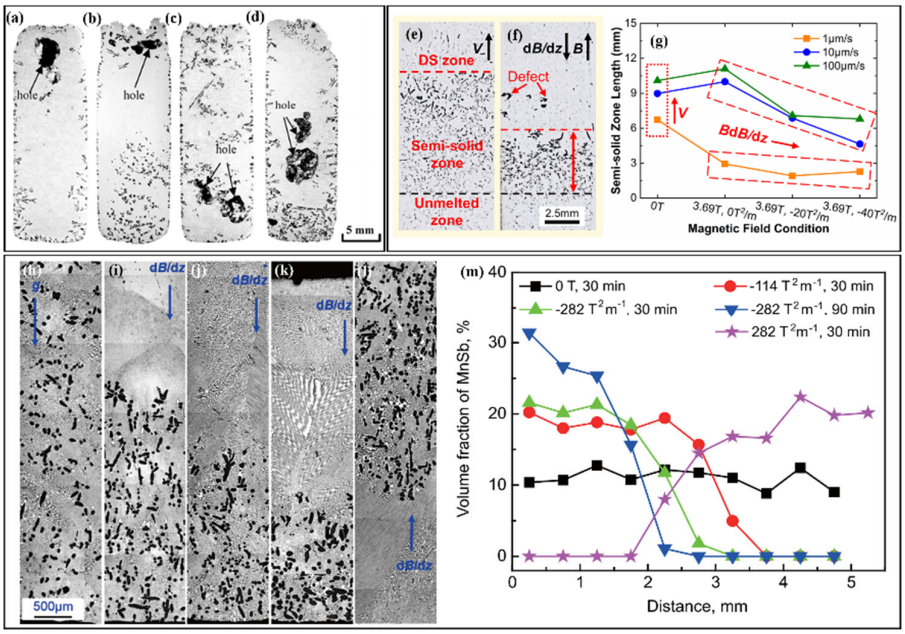

Figure 8. Macrostructures of Al-15.0wt.%Si alloy under various gradient high SMFs. (**a**) 0 T, B max position; (**b**) 8.8 T, $B(\mathrm{d}B/\mathrm{d}z)\mathrm{max} = 564\ \mathrm{T}^2/\mathrm{m}$; (**c**) 8.8 T, $B(\mathrm{d}B/\mathrm{d}z)\mathrm{max} = -564\ \mathrm{T}^2/\mathrm{m}$; (**d**) 0 T, $-B(\mathrm{d}B/\mathrm{d}z)\mathrm{max}$ position [21]. Microstructure and length of semi-solid zone of Al-1.9wt.%Fe. (**e**) Semi-solid zone at 10 μm/s, 0 T; (**f**) semi-solid zone at 10 μm/s, 3.69 T, $-40\ \mathrm{T}^2/\mathrm{m}$; (**g**) length evolution of semi-solid zone. Microstructure for Mn-89.7wt.%Sb alloys annealed in different gradient high SMFs and various annealing times [28]. (**h**) 0 T, 30 min; (**i**) $B\mathrm{d}B/\mathrm{d}z = -114\ \mathrm{T}^2/\mathrm{m}$, 30 min; (**j**) $B\mathrm{d}B/\mathrm{d}z = -282\ \mathrm{T}^2/\mathrm{m}$, 30 min; (**k**) $B\mathrm{d}B/\mathrm{d}z = -282\ \mathrm{T}^2/\mathrm{m}$, 90 min; (**l**) $B\mathrm{d}B/\mathrm{d}z = 282\ \mathrm{T}^2/\mathrm{m}$, 30 min. (**m**) Volume fraction distributions of MnSb particles along the depth from the bottom end to the top end in Mn-89.7wt.%Sb ingots solidified at various gradient high SMFs for different annealing time [8].

For instance, in the case of Al-Si alloys, primary silicon crystals were found to aggregate at the upper or lower part of the sample under the gradient high SMFs, while they only appeared at the edge of the ingots without the gradient high SMF, as shown in Figure 8a–d [21]. Directionally solidified Al-1.9wt.%Fe ETAs showed that the gradient high SMF decreased the mush zone length, particularly at low growth rates, and induced a morphological transition from eutectic instability to single-phase instability, dendrite transition, and cellular transition stages. This transition was attributed to constitutional supercooling caused by gradient high SMF, as shown in Figure 8e–g [28]. In Mn-89.7wt.%Sb hypoeutectic alloys, the migration of MnSb phases above the Curie temperature could be effectively controlled by using the gradient high SMF, indicating the potential for processing the graded metal materials, as shown in Figure 8h–m [43,60].

Overall, these findings shed light on the effect of magnetic force on the migration of solutes and particles in specific ETA systems and may have implications for designing new microstructures in a wide range of materials.

5. Magnetic Gibbs Energy during Phase Transition

5.1. Phase Transition Temperature and Nucleation Events

In Equation (5), it can be known that the SMF introduces an additional magnetic Gibbs energy to the system, which can potentially impact the thermodynamics of solidification. Ferromagnetic materials, such as Fe-C [109] and Bi-Mn [13] binary alloys, exhibit significant alterations in their thermodynamic behaviors during their phase transformation stages when exposed to a high SMF, owing to their high magnetic susceptibility. It was reported that under a 20 T high SMF, the austenite–ferrite phase transition temperature increased by approximately 20 K [78]. However, for non-ferromagnetic ETAs, the influence of high SMFs on thermodynamics remains insignificant and requires further investigation from a

theoretical and experimental standpoint. Theoretical analysis suggests that the influence of high SMFs on the liquid–solid phase transition temperature in non-ferromagnetic materials is minimal and can be disregarded [110]. Experimental measurements of liquidus and eutectic temperature of an Al-Cu alloy under 3.5 T indicated that high SMFs did not affect the phase transition temperature [111]. Other results also indicated that the solid–liquid phase transition temperature remained unchanged during the heating stage under an SMF [112,113]. A differential thermal analysis (DTA) apparatus, which was used in the SMF, was designed to find out the change of temperature as shown in Figure 7a. The sample cell consisted of a reference platinum holder and a sample platinum holder, in the bottoms of which two Pt-Pt10%Rh thermocouples were placed. DTA data then can be obtained under the SMF. The DTA of an Al-Cu hypereutectic alloy demonstrated a significant decrease in liquidus temperature during the cooling stage under a high SMF [65,113,114] (Figure 9). The decrease of liquidus temperature may be attributed to the increase of nucleation undercooling caused by changing the interfacial free energy, which acts as a barrier for the nucleation event [115]. Indeed, the shift in liquid–solid phase transition temperature indicates that the high SMF may affect the attachment process of solute atoms to the interface of the solidified solid phases. To gain a comprehensive understanding of this process, atomic-scale experiments are required.

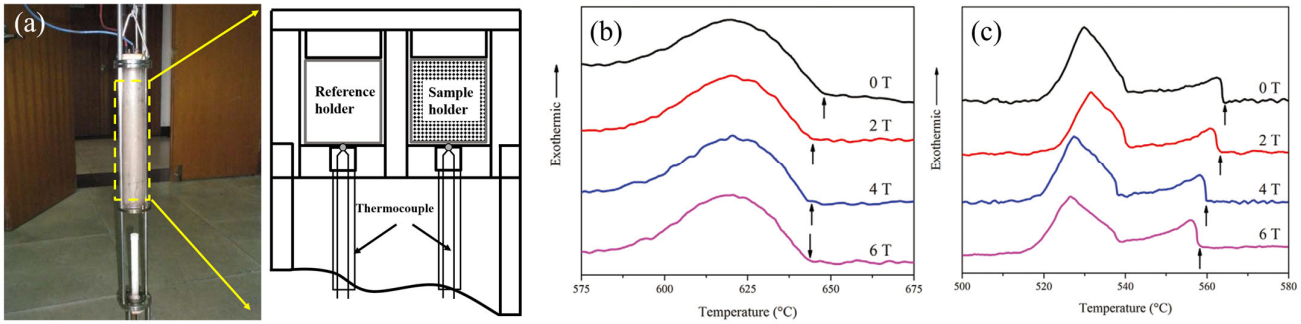

Figure 9. (**a**) DTA apparatus designed for SMF. DTA curves of the Al-Cu alloys solidified in different MFDs: (**b**) Al-4.5wt.%Cu; (**c**) Al-45wt.%Cu. Arrows indicate the nucleation temperatures of primary phases [65].

The effect of s high SMF on interfacial free energy was investigated using the grain boundary groove method [116,117]. These studies showed that the high SMF increases the interfacial free energy of the α-Al/Al-Cu system, while decreasing the interfacial free energy of the Al_2Cu/Al-Cu system, as depicted in Figure 10 [117]. The variation of interfacial free energy in these systems was explained using the magnetic dipole–dipole interaction theory. However, a complete understanding of the influence of SMF on interfacial free energy is still elusive. This is because the solid–liquid interface under the SMF is subject to TEM convection, which is absent in the absence of an SMF. Furthermore, the magnetic susceptibility and thermoelectric powers of the solid and liquid phase still lack data. To address these issues, it is then again necessary to investigate the solid–liquid layer at the atomic scale.

Al-Si alloys and pure Al have been extensively studied to investigate nucleation events in metallic systems under the influence of SMF [23,57]. Chen et al. [23] examined the solidification of Al-20wt.%Si alloys with and without a phosphorus (P) addition under the influence of an SMF. The authors evaluated the morphology and distribution of primary Si particles, as shown in Figure 11a–h. Interestingly, they observed that the grain size initially decreased and then increased with the P addition, while it continuously decreased without the P addition. Moreover, an inverse trend was observed between the average size of primary Si and the MFD, as depicted in Figure 11i, and for the primary Si per unit area (N_A), as shown in Figure 11j. The authors attributed these observations to the influence of

the SMF on both the thermodynamic nucleation event and the kinetic growth of primary Si particles.

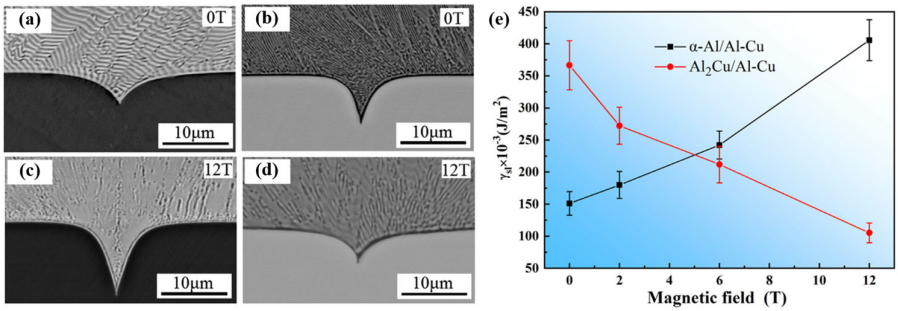

Figure 10. Typical grain boundary groove shapes under different MFDs: (**a**,**c**) α-Al/Al-Cu system in Al-30wt.%Cu alloy; (**b**,**d**) Al_2Cu/Al-Cu system in Al-35wt.%Cu alloy; (**e**) Solid–liquid interface energy of α-Al/Al-Cu and Al_2Cu/Al-Cu systems [117].

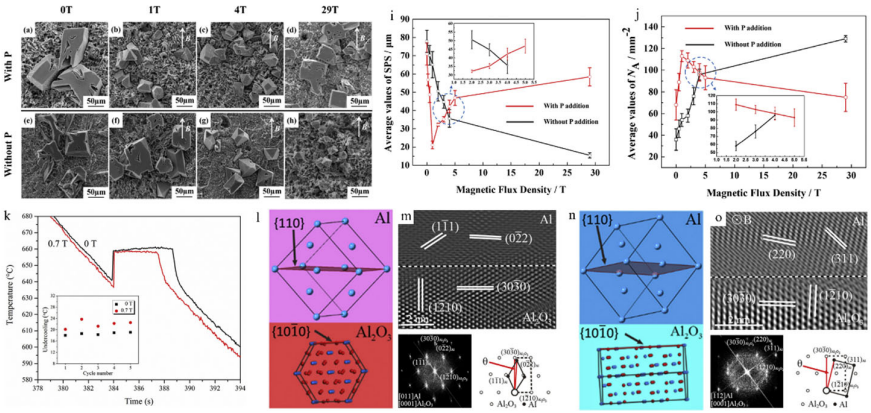

Figure 11. (**a**–**h**) SEM images of Al-20wt.%Si alloys under different MFD with and without P addition. The particles are primary Si. (**i**,**j**) Average size of primary Si (SPS) and primary Si per unit area (NA) with and without P addition under different MFD in Al-20wt.%Si alloys [23]. (**k**) Cooling curves of Al with and without the SMF. The inset is the undercooling of Al with and without the SMF for different thermal cycles. (**l**,**n**) EBSD maps and schematic illustrations of lattice matching between Al and Al_2O_3 of Al/{10$\bar{1}$0}Al_2O_3 couples in 0 T and 0.7 T, respectively. (**m**,**o**) Inverse Fast Fourier Transformation (IFFT) images and Fast Fourier Transformation (FFT) images of HRTEM with schematic indexes of FFT patterns of Al/Al_2O_3 interfaces in 0 T and 0.7 T demonstrate the angle deviation [57].

In contrast to the macroscopic observations of microstructure, Cheng et al. [57] examined the heterogeneous nucleation behavior of pure Al on an Al_2O_3 single crystal substrate under the influence of an SMF at the atomic scale. The cooling curve demonstrated that nucleation undercooling increased under the 0.7 T SMF, as shown in Figure 11k. Furthermore, lattice diagrams deduced from the EBSD map showed that the {110} plane of Al was nearly parallel to {10$\bar{1}$0} of the Al_2O_3 substrate (Figure 11l). However, an angle deviation between {10$\bar{1}$0} Al_2O_3 and {110} Al was observed under the 0.7 T SMF, as shown in Figure 11n. This angle deviation was also confirmed by the IFFT and FFT images of HRTEM with schematic indexes of FFT patterns of Al/Al_2O_3 interfaces at 0 T and 0.7 T, as presented in Figure 11m,o, respectively. Consequently, this angle deviation resulted in the decrease in nucleation undercooling. This study provides important insights into the nucleation process under the influence of SMFs at the atomic scale. However, further investigations are required to better understand the nucleation and growth mechanisms under SMFs at atomic scale.

5.2. Magnetic Orientation of Crystals Assisted by High SMF

5.2.1. Magnetic Anisotropy of Crystal

As is well known, the high orientation of a single crystal or polycrystalline structures can markedly enhance the mechanical, electrical, and optical properties of materials. In the case of ferromagnetic phases, the easily magnetized MnBi phases [51] can connect with each other and orient themselves along the direction of the SMF, owing to the attractive forces between the MnBi phases after the magnetization process. Recently, Liu et al. [118] demonstrated the generation of a strong Gaussian texture in an Fe-4.5wt.%Si alloy without rolling or heat treatment, using a high SMF of 6 T. This resulted in a significant improvement in the magnetic properties of the alloy.

In most cases, the primary phases in the ETAs often have weak magnetization properties, which are hard to magnetize. However, crystal structure with the magnetic anisotropy can also be oriented by the high SMF. If the crystal has magnetic anisotropy, the SMF can promote the crystal to grow preferentially along a specific crystal direction to keep the system at the lowest energy state. Thus, the requirement for crystal orientation is magnetic anisotropy. Taking the tetragonal structure as an example, the magnetic anisotropy energy of each crystal axis can be expressed as follows:

$$G_m^{a,b} = -\frac{V\chi_{\mathrm{a,b}}}{2\mu_0}B^2 \tag{7}$$

$$G_m^{c} = -\frac{V\chi_{\mathrm{c}}}{2\mu_0}B^2 \tag{8}$$

where $\chi_{\mathrm{a,b}}$ is the magnetic susceptibility of the a- and b-axis, and χ_{c} is the magnetic susceptibility of the c-axis. Meanwhile, the magnetic energy difference between the axes must be greater than the thermal energy [12]:

$$|\Delta G_m| = \left|\Delta G_m^C - \Delta G_m^{ab}\right| = \left|-\frac{V(x_{\mathrm{c}} - x_{\mathrm{a,b}})}{2\mu_0}\right| > k_B T \tag{9}$$

where k_{B} is the Boltzmann constant. For a solid phase entrapped in liquid, when $\Delta G_m^c > \Delta G_m^{\mathrm{a,b}}$, the c-axis is perpendicular to the SMF. In the opposite scenario, the c-axis is parallel to the SMF direction as shown in Figure 12. It is reported that crystals with shape anisotropy may also be textured by a high SMF [119].

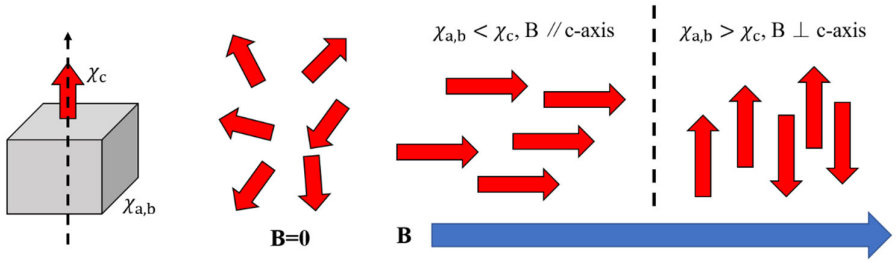

Figure 12. A schematic illustration of magnetic orientation of tetragonal crystals with different magnetic properties (χ_{a}, $\chi_{\mathrm{b}} \neq \chi_{\mathrm{c}}$) under a high SMF.

In recent years, results showed that the precipitations can be oriented under the high SMF in many ETAs, as shown in Table 2. Among these studies, Dong et al. found that the high SMF could first orient the primary MnSb phase in a Mn-Sb hypoeutectic alloy and induced the orientation of the subsequent eutectic microstructure [120]. Zheng et al. reconstructed the primary Al_2Cu phases treated by the 29 T super-high SMF using XCT and clearly observed that the Al_2Cu spatially oriented along the field direction [80].

Table 2. Summary of ETAs aligned by the high SMF.

Materials	Crystals	*B* (T)	Orientation	References
Al-Cu	Al_2Cu	1–29	c axis//B	[80,121]
Al-Fe	Al_3Fe	5	<542>//B	[122]
Al-Ni	Al_3Ni	10	c axis//B	[123]
Al-Mn	Al_6Mn	10	c axis//B	[124]
Mg-Zn/Cd-Zn	primary Zn	12	c axis//B	[38,125]
Mn-Sb	MnSb	3–11.5	c axisB	[43,120]
Bi-Mn	MnBi	2	c axis//B	[44]
Al-Si-Fe	$Al_9Si_{15}Fe$	5	Long axis of crystal⊥B	[119]

5.2.2. Magnetic Torque

In fact, as pointed out by Sugiyama [126], the influence of the SMF on the orientation process of equiaxed dendritic structures during solidification can be both thermodynamic and kinetic. For non-magnetic materials, when a particle is precipitated in a melt under SMF, magnetization M arises in it due to the imposed field, and the torque is caused by the crystal magnetic anisotropy acting on the particle. By considering the balance between the inertia, viscous, Lorenz, and magnetization forces, it has been shown that for a given radius of zinc particle, the particle can complete its rotation within one second when the MFD exceeds 1 T, and the rotation time decreases as MFD increases.

6. Eutectic High Entropy Alloy Solidified under the SMF

In past decades, EHEAs have drawn extensive interest due to their appealing physical and mechanical properties [127–129]. These multicomponent alloys with different magnetization of elements may be highly influenced by SMFs during solidification. However, few works have been performed to explore the effect of SMF on the solidification of EHEAs. In 2020, Wang et al. reported results of the effect of SMF on $AlCoCrFeNi_{2.1}$ EHEA during directional solidification, shown in Figure 13 [130]. They found that both eutectic lamellar spacing and eutectic cellular spacing decreased with the application of an SMF and the highest elongation to failure (ε_f) of the directionally solidified samples under an SMF reaches about 45 pct with an ultimate tensile strength of ~1058 MPa. They attributed the enhanced strength–ductility combination to the alignment and refinement of the microstructure under the SMF. Another AlCoCrCuFeNi high-entropy alloy was solidified under 10 T [131]. In this work, the high SMF did not induce a new type of phase (BCC plus FCC), but inhibited the precipitation of the Cu-rich FCC phase and improved the content of ferromagnetic BCC phase in the matrix phase. Therefore, the yield stress and plastic strain were improved simultaneously and the saturation magnetization value also increased. These results may provide a new way to modify the microstructures of EHEAs and enhance their mechanical properties by using SMFs in the future.

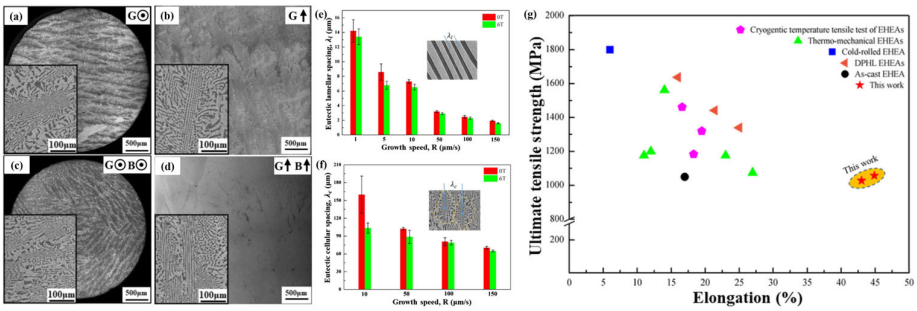

Figure 13. (**a**) Transverse and (**b**) longitudinal directional solidified microstructures in the $AlCoCrFeNi_{2.1}$ EHEAs without SMF, 20 μm/s, 0 T; (**c**,**d**) 20 μm/s, 6 T. (**e**,**f**) Effect of the growth speed and the SMF on the eutectic lamellar spacing and the eutectic cellular spacing, respectively. (**g**) Tensile properties comparison [130].

7. Industry Application

The high cost of a high SMF generator inhibits the application of high SMFs on the industrial processing of ETAs. However, a relatively low SMF is now widely used to assist materials processing. Among interesting effects caused by the SMF during solidification, magnetic braking and the TEM effects have been used for processing industry materials, such as single semiconductor crystals and electroslag-remelted steels [132,133]. To achieve larger crystals, the melt convection should be strictly controlled during crystal growth. When applying an SMF for Czochralski (CZ) growth of silicon crystals, the disturbing convective fluctuations can be suppressed and the impurity transport in the melt is also minimized, resulting in low oxygen concentration [132]. Now, during the electroslag-remelted Cr12MoV die steel process, an SMF is a powerful way to refine the microstructure [133]. Figure 14a is the schematic diagram of the remelting device, a transverse SMF was applied to the solid–liquid interface to produce a TEM force and bring TEM convection, which refined the primary dendrite and eutectic carbides (Figure 14b,c) and resulted in a homogeneous hardness (Figure 14d,e).

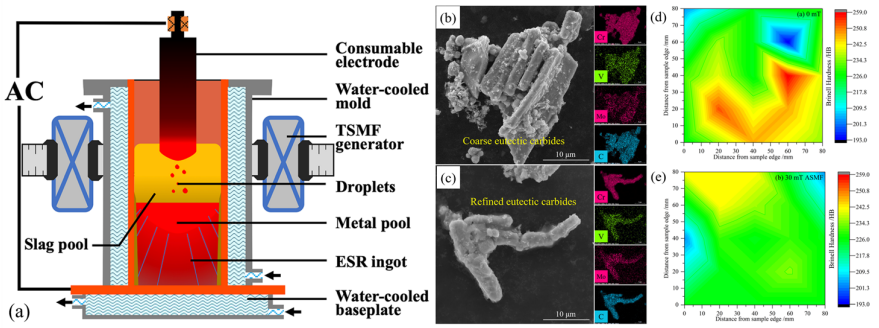

Figure 14. (**a**) Schematic diagram of the remelting device, TSMF is the transverse SMF and ESR is the electroslag-remelted. (**b**,**c**) Three-dimensional morphology of the electrolytically extracted eutectic carbides under 0 T and 30 mT, respectively. (**d**,**e**) Hardness distribution on the transverse sections of ESR ingots under 0 T and 30 mT [133].

8. Summary and Perspective

There exist two distinct avenues through which SMF can influence the solidification behavior of ETAs, namely through force and energy. In this review, we highlight recent progress in this field, which can be summarized as follows:

(1) Magnetic braking effect: The SMF can significantly reduce or even eliminate melt convections, thereby promoting diffusion-limited crystal growth. This can lead to the production of high-quality single crystals.

(2) TEM effect: The interaction between the thermoelectric current near the solid–liquid interface and the applied SMF generates a TEM force, which can influence the atomic transport behavior at the interface. Once this force is greater than a critical value, dendrites can be broken and fragments can be migrated. As a result, a CET event happens. Thus, TEM convection can not only modify the morphology of the solid–liquid interface and change solute distribution, but also refine the microstructure. Ex situ and in situ observation of the solidification process have been conducted under the weak SMF to reveal the TEM effect on the evolution of microstructure.

(3) Gradient high SMF effect: The gradient magnetic force induced by the SMF can effectively control the migration of solute and primary crystals, making it useful for processing graded metal materials, removing Fe-rich intermetallic compounds in recycled aluminum alloys, and levitating materials.

(4) Magnetic Gibbs energy effect: The high SMF can influence the phase transition of during solidification, which may be attributed to the change of solid–liquid interfacial free energy.

(5) Magnetic torque effect: Crystals with magnetic anisotropy in their unit cell can be oriented by high SMF. This is for the sake of the magnetic torque on the crystal and leads to the rotation of the crystal along the direction of the SMF. The orientation efficiency mainly depends on the crystal size and MFD.
(6) Effect on EHEAs: The high SMF can effectively affect the microstructures of EHEAs, which provides a potential way to enhance their mechanical properties.

Despite these promising effects, several scientific problems remain unresolved. For example, in situ observation of solidification under high SMFs is lacking, which would enable a better understanding of metallic crystal growth. Additionally, the metallic crystals' growth under diffusion-limited and microgravity conditions simulated by the high SMF on the ground requires further investigation. Moreover, the influence of SMFs on the physical parameters of ETAs, such as magnetic susceptibility, interface energy, diffusion coefficient, and dynamic viscosity, is still ambiguous and requires precise measuring equipment. Furthermore, while most studies have focused on the microstructural evolution of solidification, atomic-scale studies are necessary to understand the attachment of dissolvent elements in the solid–liquid interface. Finally, research is needed to determine how to use the SMF to design solidified structures of materials with excellent physical and chemical properties.

Author Contributions: Conceptualization, writing—original draft preparation, H.C. and W.L.; writing—review and editing, T.Z.; investigation, H.C. and M.F.; supervision, T.Z., B.Z. and Y.Z.; project administration, T.Z. and Y.Z.; funding acquisition, Y.Z. All authors have read and agreed to the published version of the manuscript.

Funding: This research was funded by Natural Science Foundation of Shanghai (21ZR1424400), National Natural Science Foundation of China (U1732276), Changjiang Scholars Program of China, China Association for Science and Technology Young Talent Support Project.

Data Availability Statement: Data can be made available by contacting the corresponding authors.

Conflicts of Interest: The authors declare no conflict of interest.

References

1. Chang, I.; Cai, Q. From simple binary to complex multicomponent eutectic alloys. *Prog. Mater. Sci.* **2022**, *123*, 100779. [CrossRef]
2. Khorasani, M.; Ghasemi, A.; Leary, M.; Sharabian, E.; Cordova, L.; Gibson, I.; Downing, D.; Bateman, S.; Brandt, M.; Rolfe, B. The effect of absorption ratio on meltpool features in laser-based powder bed fusion of IN718. *Opt. Laser Technol.* **2022**, *153*, 108263. [CrossRef]
3. Kim, S.H.; Yeon, S.-M.; Lee, J.H.; Kim, Y.W.; Lee, H.; Park, J.; Lee, N.-K.; Choi, J.P.; Aranas, C.; Lee, Y.J.; et al. Additive manufacturing of a shift block via laser powder bed fusion: The simultaneous utilisation of optimised topology and a lattice structure. *Virtual Phys. Prototyp.* **2020**, *15*, 460–480. [CrossRef]
4. Räbiger, D.; Zhang, Y.; Galindo, V.; Franke, S.; Willers, B.; Eckert, S. The relevance of melt convection to grain refinement in Al-Si alloys solidified under the impact of electric currents. *Acta Mater.* **2014**, *79*, 327–338. [CrossRef]
5. Abou-Khalil, L.; Salloum-Abou-Jaoude, G.; Reinhart, G.; Pickmann, C.; Zimmermann, G.; Nguyen-Thi, H. Influence of gravity level on Columnar-to-Equiaxed Transition during directional solidification of Al-20wt.%Cu alloys. *Acta Mater.* **2016**, *110*, 44–52. [CrossRef]
6. Wang, S.; Kang, J.; Guo, Z.; Lee, T.L.; Zhang, X.; Wang, Q.; Deng, C.; Mi, J. In situ high speed imaging study and modelling of the fatigue fragmentation of dendritic structures in ultrasonic fields. *Acta Mater.* **2019**, *165*, 388–397. [CrossRef]
7. Sun, Z.H.I.; Guo, M.; Vleugels, J.; Van der Biest, O.; Blanpain, B. Processing of non-ferromagnetic materials in strong static magnetic field. *Curr. Opin. Solid State Mater. Sci.* **2013**, *17*, 193–201. [CrossRef]
8. Liu, T.; Wang, Q.; Yuan, Y.; Wang, K.; Li, G. High-gradient magnetic field-controlled migration of solutes and particles and their effects on solidification microstructure: A review. *Chin. Phys. B* **2018**, *27*, 118103. [CrossRef]
9. Vives, C.; Perry, C. Solidification of a pure metal in the presence of a stationary magnetic field. *Int. Commun. Heat Mass Transf.* **1986**, *13*, 253–263. [CrossRef]
10. Vives, C.; Perry, C. Transfer-effects of magnetially damped convection during the controlled solidification of metals and alloys. *Int. J. Heat Mass Transf.* **1987**, *30*, 479–496. [CrossRef]
11. Yasuda, H.; Ohnaka, I.; Ninomiya, Y.; Ishii, R.; Fujita, S.; Kishio, K. Levitation of metallic melt by using the simultaneous imposition of the alternating and the static magnetic fields. *J. Cryst. Growth* **2004**, *260*, 475–485. [CrossRef]

12. Asai, S.; Sassa, K.-S.; Tahashi, M. Crystal orientation of non-magnetic materials by imposition of a high magnetic field. *Sci. Technol. Adv. Mater.* **2016**, *4*, 455–460. [CrossRef]
13. Koyama, K.; Mitsui, Y.; Choi, E.S.; Ikehara, Y.; Palm, E.C.; Watanabe, K. Change of the equilibrium state of ferromagnetic MnBi by high magnetic fields. *J. Alloys Compd.* **2011**, *509*, L78–L80. [CrossRef]
14. Li, X.; Ren, Z.; Fautrelle, Y. Effect of a high axial magnetic field on the microstructure in a directionally solidified Al-Al_2Cu eutectic alloy. *Acta Mater.* **2006**, *54*, 5349–5360. [CrossRef]
15. Li, X.; Ren, Z.; Fautrelle, Y. The spiral growth of lamellar eutectics in a high magnetic field during the directional solidification process. *Scr. Mater.* **2007**, *56*, 505–508. [CrossRef]
16. Li, X.; Fautrelle, Y.; Ren, Z. Influence of thermoelectric effects on the solid-liquid interface shape and cellular morphology in the mushy zone during the directional solidification of Al-Cu alloys under a magnetic field. *Acta Mater.* **2007**, *55*, 3803–3813. [CrossRef]
17. Huang, C.; Shuai, S.; Wang, P.; Liu, X.; Wang, J.; Ren, Z. The effect of static magnetic field on solid-liquid interfacial free energy of Al-Cu alloy system. *Scr. Mater.* **2020**, *187*, 232–236. [CrossRef]
18. Beaugnon, E.; Bourgault, D.; Braithwaite, D.; de Rango, P.; Perrier de la Bathie, R.; Sulpice, A.; Tournier, R. Material processing in high static magnetic field. A review of an experimental study on levitation, phase separation, convection and texturation. *J. Phys. I* **1993**, *3*, 399–421. [CrossRef]
19. Lehmann, P.; Moreau, R.; Camel, D.; Bolcato, R. Modification of interdendritic convection in directional solidification by a uniform magnetic field. *Acta Mater.* **1998**, *46*, 4067–4079. [CrossRef]
20. Zuo, X.; Zhao, C.; Niu, R.; Wang, E.; Han, K. Microstructural dependence of magnetoresistance in CuAg alloy solidified with high magnetic field. *J. Mater. Process. Technol.* **2015**, *224*, 208–212. [CrossRef]
21. Wang, Q.; Wang, C.J.; Liu, T.; Wang, K.; He, J.C. Control of solidified structures in aluminum-silicon alloys by high magnetic fields. *J. Mater. Sci.* **2007**, *42*, 10000–10006. [CrossRef]
22. Liu, T.; Wang, Q.; Zhang, H.-W.; Lou, C.-S.; Nakajima, K.; He, J.-C. Effects of high magnetic fields on solidification microstructure of Al-Si alloys. *J. Mater. Sci.* **2010**, *46*, 1628–1634. [CrossRef]
23. Chen, X.; Zhong, Y.; Zheng, T.; Shen, Z.; Wang, J.; Fan, L.; Zhai, Y.; Peng, M.; Zhou, B.; Ren, W.; et al. Refinement of primary Si in the bulk solidified Al-20wt.%Si alloy assisting by high static magnetic field and phosphorus addition. *J. Alloys Compd.* **2017**, *714*, 39–46. [CrossRef]
24. Wang, Q.; Lou, C.; Liu, T.; Pang, X.; Nakajima, K.; He, J. Effects of Uniform and Gradient High Magnetic Fields on Gravity Segregation in Aluminum Alloys. *ISIJ Int.* **2009**, *49*, 1094–1097. [CrossRef]
25. Li, L.; Zhang, Y.; Esling, C.; Jiang, H.; Zhao, Z.; Zuo, Y.; Cui, J. Influence of a high magnetic field on the precipitation behavior of the primary Al3Fe phase during the solidification of a hypereutectic Al-3.31wt.%Fe alloy. *J. Cryst. Growth* **2012**, *339*, 61–69. [CrossRef]
26. Wu, M.; Liu, T.; Dong, M.; Sun, J.; Dong, S.; Wang, Q. Directional solidification of Al-8 wt. %Fe alloy under high magnetic field gradient. *J. Appl. Phys.* **2017**, *121*, 064901. [CrossRef]
27. Tang, P.; Tian, Y.; Liu, S.; Lv, Y.; Xie, Y.; Yan, J.; Liu, T.; Wang, Q. Microstructure development in eutectic Al-Fe alloy during directional solidification under high magnetic fields at different growth velocities. *J. Mater. Sci.* **2021**, *56*, 16134–16144. [CrossRef]
28. Yan, J.; Liu, T.; Wang, M.; Sun, J.; Dong, S.; Zhao, L.; Wang, Q. Constitutional supercooling and corresponding microstructure transition triggered by high magnetic field gradient during directional solidification of Al-Fe eutectic alloy. *Mater. Charact.* **2022**, *188*, 111920. [CrossRef]
29. Xiao, Y.; Liu, T.; Tong, Y.; Dong, M.; Li, J.; Wang, J.; Wang, Q. Microstructure evolution of peritectic Al-18at.%Ni alloy directionally solidified in high magnetic fields. *J. Mater. Sci. Technol.* **2021**, *76*, 51–59. [CrossRef]
30. Shuai, S.; Lin, X.; Dong, Y.; Hou, L.; Liao, H.; Wang, J.; Ren, Z. Three dimensional dendritic morphology and orientation transition induced by high static magnetic field in directionally solidified Al-10 wt.%Zn alloy. *J. Mater. Sci. Technol.* **2019**, *35*, 1587–1592. [CrossRef]
31. Moreau, R.; Laskar, O.; Tanaka, M.; Camel, D. Thermoelectric magnetohydrodynamic effects on solidification of metallic alloys in the dendritic regime. *Mater. Sci. Eng. A* **1993**, *173*, 93–100. [CrossRef]
32. Shen, Z.; Peng, M.; Zhu, D.; Zheng, T.; Zhong, Y.; Ren, W.; Li, C.; Xuan, W.; Ren, Z. Evolution of the microstructure and solute distribution of Sn-10wt.%Bi alloys during electromagnetic field-assisted directional solidification. *J. Mater. Sci. Technol.* **2019**, *35*, 568–577. [CrossRef]
33. Shen, Z.; Zhou, B.; Zhong, Y.; Zheng, T.; Ren, W.; Lei, Z.; Ren, Z. Revealing influence mechanism of a transverse static magnetic field on the refinement of primary dendrite spacing during directional solidification. *J. Cryst. Growth* **2019**, *517*, 54–58. [CrossRef]
34. Song, H.; Tewari, S.N.; de Groh, H.C., III. Convection during thermally unstable solidification of Pb-Sn in a magnetic field. *Metall. Mater. Trans. A* **1996**, *27*, 1095–1110. [CrossRef]
35. Kaldre, I.; Fautrelle, Y.; Etay, J.; Bojarevics, A.; Buligins, L. Thermoelectric current and magnetic field interaction influence on the structure of directionally solidified Sn-10wt.%Pb alloy. *J. Alloys Compd.* **2013**, *571*, 50–55. [CrossRef]
36. Du, D.; Hou, L.; Gagnoud, A.; Ren, Z.; Fautrelle, Y.; Cao, G.; Li, X. Effect of an axial high magnetic field on Sn dendrite morphology of Pb-Sn alloys during directional solidification. *J. Alloys Compd.* **2014**, *588*, 190–198. [CrossRef]
37. Li, L.; Zhang, R.; Ban, C.; Zhang, H.; Liu, T.; Zhang, H.; Wang, X.; Esling, C.; Cui, J. Growth behavior of Zn-rich phase in Zn-Mg alloy under a high magnetic field. *Mater. Charact.* **2019**, *151*, 191–202. [CrossRef]

38. Li, L.; Ban, C.; Bi, Y.; Zhang, R.; Zhang, H.; Liu, T.; Zhu, Q.; Zuo, Y.; Wang, X.; Cui, J. A crystallographic study on the growth of Laves phase MgZn2 during the solidification process of Zn-Mg alloy under a high magnetic field. *J. Mater. Sci.* **2018**, *53*, 15181–15195. [CrossRef]
39. Zhai, C.; Luo, Q.; Cai, Q.; Guan, R.; Li, Q. Thermodynamically analyzing the formation of $Mg_{12}Nd$ and $Mg_{41}Nd_5$ in Mg-Nd system under a static magnetic field. *J. Alloys Compd.* **2019**, *773*, 202–209. [CrossRef]
40. He, Y.; Li, J.; Li, L.; Wang, J.; Yildiz, E.; Beaugnon, E. Magnetic-field-induced chain-like assemblies of the primary phase during non-equilibrium solidification of a Co-B eutectic alloy: Experiments and modeling. *J. Alloys Compd.* **2020**, *815*, 152446. [CrossRef]
41. Bu, F.; Zhang, Y.; Liu, H.; Wang, J.; Beaugnon, E.; Li, J.; He, Y. Magnetic field intensity dependent microstructure evolution and recrystallization behavior in a Co-B eutectic alloy. *J. Mater. Sci. Technol.* **2023**, *138*, 93–107. [CrossRef]
42. Wang, J.; He, Y.; Li, J.; Kou, H.; Beaugnon, E. Strong magnetic field effect on the nucleation of a highly undercooled Co-Sn melt. *Sci. Rep.* **2017**, *7*, 4958. [CrossRef]
43. Liu, T.; Wang, Q.; Gao, A.; Zhang, C.; Li, D.; He, J. Crystal orientation and grain alignment in a hypoeutectic Mn-Sb alloy under high magnetic field conditions. *J. Alloys Compd.* **2009**, *481*, 755–760. [CrossRef]
44. Li, X.; Ren, Z.; Fautrelle, Y. Effect of high magnetic fields on the microstructure in directionally solidified Bi-Mn eutectic alloy. *J. Cryst. Growth* **2007**, *299*, 41–47. [CrossRef]
45. Cao, J.; Shuai, S.; Huang, C.; Hu, T.; Chen, C.; Wang, J.; Ren, Z. 4D synchrotron X-ray tomographic study of the influence of transverse magnetic field on iron intermetallic compounds precipitation behavior during solidification of Al-Si-Fe alloy. *Intermetallics* **2022**, *143*, 107471. [CrossRef]
46. Du, D.; Fautrelle, Y.; Ren, Z.; Moreau, R.; Li, X. Effect of a high magnetic field on the growth of ternary Al-Cu-Ag alloys during directional solidification. *Acta Mater.* **2016**, *121*, 240–256. [CrossRef]
47. Du, D.; Dong, A.; Shu, D.; Zhu, G.; Sun, B.; Li, X. Microstructure and Crystallization Evolution of Directionally Solidified Al-Cu-Si Alloys with the Assistance of a Static Magnetic Field. *Metall. Mater. Trans. A* **2022**, *143*, 107471. [CrossRef]
48. Liu, H.; Xuan, W.; Xie, X.; Yu, J.; Wang, J.; Li, X.; Zhong, Y.; Ren, Z.; Wang, H.; Dai, Y. Effect of a high magnetic field on solidification structure in directionally solidified NiAl-Cr(Mo)-Hf eutectic alloy. *J. Alloys Compd.* **2018**, *737*, 74–82. [CrossRef]
49. Utech, H.P.; Flemings, M.C. Elimination of Solute Banding in Indium Antimonide Crystals by Growth in a Magnetic Field. *J. Appl. Phys.* **1966**, *37*, 2021–2024. [CrossRef]
50. Shercliff, J.A. Thermoelectric magnetohydrodynamics. *J. Fluid Mech.* **2006**, *91*, 231–251. [CrossRef]
51. Zheng, T.; Zhong, Y.; Dong, L.; Zhou, B.; Ren, Z.; Debray, F.; Beaugnon, E. Orientation of Magnetized MnBi in a Strong Static Magnetic Field. *Metall. Mater. Trans. A* **2018**, *49*, 1981–1985. [CrossRef]
52. Botton, V.; Lehmann, P.; Bolcato, R.; Moreau, R.; Haettel, R. Measurement of solute diffusivities. Part II. Experimental measurements in a convection-controlled shear cell. Interest of a uniform magnetic field. *Int. J. Heat Mass Transf.* **2001**, *44*, 3345–3357. [CrossRef]
53. Miyake, T.; Inatomi, Y.; Kuribayashi, K. Measurement of Diffusion Coefficient in Liquid Metal under Static Magnetic Field. *Jpn. J. Appl. Phys.* **2002**, *41*, L811–L813. [CrossRef]
54. Cahoon, J.R.; Youdelis, W.V. Application of a magnetic field to suppress convective velocities during liquid diffusion. *Can. Metall. Q.* **2013**, *8*, 39–40. [CrossRef]
55. Liu, Y.; Lin, W.; Zhou, B.; Zheng, T.; Zhong, Y.; Zhang, L. A novel gravity-assisted automatic docking device for studying diffusion in liquid metal melts assisted by a strong static magnetic field. *Rev. Sci. Instrum.* **2021**, *92*, 094903. [CrossRef] [PubMed]
56. Zhou, B.; Lin, W.; Liu, Y.; Cai, H.; Zheng, T.; Liu, C.; Zhong, Y. Atomic diffusion in liquid Al-Cu melt under static magnetic fields. *J. Appl. Phys.* **2022**, *132*, 165106. [CrossRef]
57. Cheng, N.; Guo, R.; Shuai, S.; Wang, J.; Xia, M.; Li, J.; Ren, Z.; Li, J.; Wang, Q. Influence of static magnetic field on the heterogeneous nucleation behavior of Al on single crystal Al_2O_3 substrate. *Materialia* **2020**, *13*, 100847. [CrossRef]
58. Wang, P.; Shuai, S.; Huang, C.; Liu, X.; Fu, Y.; Wang, J.; Ren, Z. Revealing the influence of high magnetic field on the solute distribution during directional solidification of Al-Cu alloy. *J. Mater. Sci. Technol.* **2021**, *88*, 226–232. [CrossRef]
59. He, S.Y.; Li, C.J.; Guo, R.; Xuan, W.D.; Wang, J.; Ren, Z.M. Evolution of microsegregation in directionally solidified Al-Cu alloys under steady magnetic field. *J. Alloys Compd.* **2019**, *800*, 41–49. [CrossRef]
60. Liu, T.; Wang, Q.; Gao, A.; Zhang, C.; Wang, C.; He, J. Fabrication of functionally graded materials by a semi-solid forming process under magnetic field gradients. *Scr. Mater.* **2007**, *57*, 992–995. [CrossRef]
61. Lin, W.; Zhou, B.; Liu, Y.; Guo, X.; Zheng, T.; Zhong, Y.; Zhang, L.; Zhang, Q.; Wang, Q. Dendrite morphology in Al-20wt.%Cu hypoeutectic alloys in 24 T high magnetic field quantified by ex-situ X-ray tomography. *J. Alloys Compd.* **2022**, *918*, 165679. [CrossRef]
62. Li, X.; Fautrelle, Y.; Ren, Z. Morphological instability of cell and dendrite during directional solidification under a high magnetic field. *Acta Mater.* **2008**, *56*, 3146–3161. [CrossRef]
63. He, S.Y.; Zhan, T.J.; Li, C.J.; Xuan, W.D.; Wang, J.; Ren, Z.M. Enhanced Dendrite Coarsening and Microsegregation in Al-Cu Alloy under a Steady Magnetic Field. *Mater. Trans.* **2019**, *60*, 1921–1927. [CrossRef]
64. Lou, C.; Wang, Q.; Wang, C.; Liu, T.; Nakajima, K.; He, J. Migration and rotation of TiAl3 particles in an Al-melt solidified under high magnetic field conditions. *J. Alloys Compd.* **2009**, *472*, 225–229. [CrossRef]
65. Guo, R.; Li, C.; He, S.; Wang, J.; Xuan, W.; Li, X.; Zhong, Y.; Ren, Z. Effect of steady magnetic field on undercooling of Al-Cu alloy melts. *Europhys. Lett.* **2019**, *126*, 46001. [CrossRef]

66. Zheng, T.; Shi, P.; Shen, Z.; Zhou, B.; Lin, W.; Liang, X.; Liu, W.; Chen, X.; Zhong, Y.; Wang, H.; et al. Diffusion-controlled mechanical property-enhancement of Al-20wt.%Si ribbon annealed under high static magnetic fields, from the microscale to the atomic scale. *Mater. Des.* **2020**, *188*, 108476. [CrossRef]
67. Liu, Y.; Lin, W.; Zhou, B.; Guo, X.; Cai, H.; Zheng, T.; Ding, B.; Zhong, Y.; Zhang, L. Ex-situ study of diffusion in liquid Al-Cu melts under a transverse magnetic field using X-ray imaging. *Philos. Mag. Lett.* **2022**, *102*, 151–159. [CrossRef]
68. Lin, W.; Liu, Y.; Zhou, B.; Cai, H.; Shen, Z.; Ren, W.; Lei, Z.; Liu, C.; Zheng, T.; Zhong, Y.; et al. Synthesis of single metallic crystal in microgravity simulated by static magnetic field. *Scr. Mater.* **2022**, *221*, 114969. [CrossRef]
69. Zhou, B.; Lin, W.; Shen, Z.; Zheng, T.; Zhong, Y.; Beaugnon, E.; Debray, F.; Zhang, L.; Wang, H.; Wang, Q. Growth dynamics of the segregated phase in Zn-6wt.%Bi immiscible alloy superheated in super high static magnetic field. *J. Alloys Compd.* **2021**, *879*, 160410. [CrossRef]
70. Zhou, B.; Guo, X.; Lin, W.; Liu, Y.; Guo, Y.; Zheng, T.; Zhong, Y.; Wang, H.; Wang, Q. Effect of Vertical High Magnetic Field on the Morphology of Solid-Liquid Interface during the Directional Solidification of Zn-2wt.%Bi Immiscible Alloy. *Metals* **2022**, *12*, 875. [CrossRef]
71. Zhou, B.; Lin, W.; Guo, Y.; Zheng, T.; Zhong, Y.; Zhang, L.; Zhang, Q. Tailoring homogeneous immiscible alloy via magneto-Archimedes levitation. *Scr. Mater.* **2023**, *226*, 115268. [CrossRef]
72. Guo, Y.; Qi, W.; Xia, Z.; Lin, W.; Liu, C.; Shi, P.; Li, Q.; Shen, Z.; Ding, B.; Zheng, T.; et al. Refinement of Eutectic Carbides in M2 High Speed Steel by Adjusting Magnetic Flux Density During Magnetic Controlled ESR Process. *Metall. Mater. Trans. B* **2022**, *53*, 3384–3395. [CrossRef]
73. Guo, Y.; Qi, W.; Xia, Z.; Zhao, X.; Li, Q.; Liu, C.; Ding, B.; Shen, Z.; Zheng, T.; Zhong, Y. Morphology tailoring of metal pool and eutectic carbides in magnetic-controlled electroslag remelted M2 high-speed steel. *J. Mater. Res. Technol.* **2022**, *16*, 1122–1135. [CrossRef]
74. Qi, W.; Guo, Y.; Ma, C.; Xia, Z.; Li, Q.; Liu, C.; Shi, P.; Ding, B.; Shen, Z.; Zheng, T.; et al. Multi-Stage Enhanced Removal of Inclusions During Electroslag Remelting Process by a Static Magnetic Field. *Steel Res. Int.* **2022**, *93*, 2200273. [CrossRef]
75. Alboussiere, T.; Moreau, R.; Camel, D. Influence of a magnetic-field on the solidification of metallic alloys. *C. R. Acad. Sci.* **1991**, *313*, 749–755. Available online: https://gallica.bnf.fr/ark:/12148/bpt6k63186794/f761.item# (accessed on 22 April 2023).
76. Sun, Z.; Vleugels, M.G.J.; Van Der Biest, O.; Blanpain, B. Numerical Calculations on Inclusion Removal From Liquid Metals Under Strong Magnetic Fields. *Prog. Electromagn. Res.* **2009**, *98*, 359–373. [CrossRef]
77. Beaugnon, E.; Tournier, R. Levitation of organic materials. *Nature* **1991**, *349*, 470. [CrossRef]
78. Joo, H.D.; Choi, J.K.; Kim, S.U.; Shin, N.S.; Koo, Y.M. An effect of a strong magnetic field on the phase transformation in plain carbon steels. *Metall. Mater. Trans. A* **2004**, *35*, 1663–1668. [CrossRef]
79. Li, Z.; Chen, L.; Meng, S.; Guo, L.; Huang, J.; Liu, Y.; Wang, W.; Chen, X. Field and temperature dependence of intrinsic diamagnetism in graphene: Theory and experiment. *Phys. Rev. B* **2015**, *91*, 094429. [CrossRef]
80. Zheng, T.; Zhou, B.; Wang, J.; Shuai, S.; Zhong, Y.; Ren, W.; Ren, Z.; Debray, F.; Beaugnon, E. Compression properties enhancement of Al-Cu alloy solidified under a 29 T high static magnetic field. *Mater. Sci. Eng. A* **2018**, *733*, 170–178. [CrossRef]
81. Cai, B.; Kao, A.; Boller, E.; Magdysyuk, O.V.; Atwood, R.C.; Vo, N.T.; Pericleous, K.; Lee, P.D. Revealing the mechanisms by which magneto-hydrodynamics disrupts solidification microstructures. *Acta Mater.* **2020**, *196*, 200–209. [CrossRef]
82. Wang, J.; Fautrelle, Y.; Nguyen-Thi, H.; Mangelinck-Noel, N.; Salloum Abou Jaoude, G.; Kaldre, I.; Bojarevics, A.; Buligins, L. Thermoelectric magnetic force acting on the solid during directional solidification under a static magnetic field. *Appl. Phys. Lett.* **2012**, *101*, 251904. [CrossRef]
83. Fautrelle, Y.; Wang, J.; Du, D.; Li, X.; Ren, Z. High Magnetic Field Processing of Metal Alloys. In *Solidification Processing of Metallic Alloys Under External Fields*; Eskin, D., Mi, J., Eds.; Springer: Cham, Switzerland, 2018; Volume 273. [CrossRef]
84. Gelfgat, A.Y.; Bar-Yoseph, P.Z.; Solan, A. Effect of axial magnetic field on three-dimensional instability of natural convection in a vertical Bridgman growth configuration. *J. Cryst. Growth* **2001**, *230*, 63–72. [CrossRef]
85. Xu, B.; Li, B.Q.; Stock, D.E. An experimental study of thermally induced convection of molten gallium in magnetic fields. *Int. J. Heat Mass Transf.* **2006**, *49*, 2009–2019. [CrossRef]
86. Chen, L.; Liu, B.Q.; Ni, M.J. Study of natural convection in a heated cavity with magnetic fields normal to the main circulation. *Int. J. Heat Mass Transf.* **2018**, *127*, 267–277. [CrossRef]
87. Mao, S.; Wang, X.; Sun, D.; Wang, J. Numerical modeling of dendrite growth in a steady magnetic field using the two relaxation times lattice Boltzmann-phase field model. *Comp. Mater. Sci.* **2022**, *204*, 111149. [CrossRef]
88. Yu, H.; Tandon, K.N.; Cahoon, J.R. Solidification of Hypereutectic Al-38 Wt Pct Cu Alloy in Microgravity and in Unit Gravity. *Metall. Mater. Trans. A* **1997**, *28*, 1245–1250. [CrossRef]
89. Li, L.; Xu, B.; Tong, W.P.; He, L.Z.; Ban, C.Y.; Zhang, H.; Zuo, Y.B.; Zhu, Q.F.; Cui, J.Z. Directional growth behavior of α(Al) dendrites during concentration-gradient-controlled solidification process in static magnetic field. *Trans. Nonferrous Met. Soc. China* **2015**, *25*, 2438–2445. [CrossRef]
90. Li, L.; Xu, B.; Tong, W.P.; Zhang, H.; Ban, C.Y.; He, L.Z.; Zhao, Z.H.; Zuo, Y.B.; Zhu, Q.F.; Cui, J.Z. Directional Growth of Tin Crystals Controlled by Combined Solute Concentration Gradient Field and Static Magnetic Field. *Acta Metall. Sin.* **2015**, *28*, 725–732. [CrossRef]
91. Asai, S. Rencent development and prospect of electromagnetic processing of materials. *Sci. Technol. Adv. Mater.* **2000**, *1*, 191–200. [CrossRef]

92. Fautrelle, Y.; Wang, J.; Salloum-Abou-Jaoude, G.; Abou-Khalil, L.; Reinhart, G.; Li, X.; Ren, Z.M.; Nguyen-Thi, H. Thermo-Electric-Magnetic Hydrodynamics in Solidification: In Situ Observations and Theory. *JOM* **2018**, *70*, 764–771. [CrossRef]
93. Khine, Y.Y.; Walker, J.S. Thermoelectric magnetohydrodynamic effects during Bridgman semiconductor crystal growth with a uniform axial magnetic field. *J. Cryst. Growth* **1998**, *183*, 150–158. [CrossRef]
94. Li, X.; Fautrelle, Y.; Ren, Z.; Gagnoud, A.; Moreau, R.; Zhang, Y.; Esling, C. Effect of a high magnetic field on the morphological instability and irregularity of the interface of a binary alloy during directional solidification. *Acta Mater.* **2009**, *57*, 1689–1701. [CrossRef]
95. Li, X.; Gagnoud, A.; Ren, Z.; Fautrelle, Y.; Moreau, R. Investigation of thermoelectric magnetic convection and its effect on solidification structure during directional solidification under a low axial magnetic field. *Acta Mater.* **2009**, *57*, 2180–2197. [CrossRef]
96. Li, X.; Zhang, Y.; Fautrelle, Y.; Ren, Z.; Esling, C. Experimental evidence for liquid-solid interface instability caused by the stress in the solid during directional solidification under a strong magnetic field. *Acta Mater.* **2009**, *60*, 489–492. [CrossRef]
97. Inoue, K.; Yasuda, H.; Minami, Y.; Nagira, T.; Yoshiya, M.; Uesugi, K.; Umetani, K. Direct observation of thermoelectric magnetic convection in unidirectionally solidified Al-Cu alloys. *J. Iron Steel Res. Int.* **2012**, *198*, 34–39. [CrossRef]
98. Wang, J.; Fautrelle, Y.; Nguyen-Thi, H.; Salloum Abou Jaoude, G.; Reinhart, G.; Mangelinck-Noël, N.; Kaldre, I. Thermoelectric magnetic flows in melt during directional solidification. *Appl. Phys. Lett.* **2014**, *104*, 121916. [CrossRef]
99. Shen, Z.; Zhou, B.; Zhong, Y.; Dong, L.; Wang, H.; Fan, L.; Zheng, T.; Li, C.; Ren, W.; Xuan, W.; et al. An Electromagnetic Compounding Technique for Counteracting the Thermoelectric Magnetic Effect During Directional Solidification Under a Transverse Static Magnetic Field. *Metall. Mater. Trans. A* **2018**, *49*, 3373–3382. [CrossRef]
100. Wang, J.; Yue, S.; Fautrelle, Y.; Lee, P.D.; Li, X.; Zhong, Y.; Ren, Z. Refinement and growth enhancement of Al_2Cu phase during magnetic field assisting directional solidification of hypereutectic Al-Cu alloy. *Sci. Rep.* **2016**, *6*, 24585. [CrossRef]
101. Liu, T.; Miao, L.; Wang, K.; Wang, L.; Sun, J.; Wang, Q. High magnetic-field-induced solute interception among dendrite arms in the mushy zone of a Mn-Sb alloy. *J. Appl. Phys.* **2018**, *124*, 045901. [CrossRef]
102. Zhu, L.; Han, C.; Hou, L.; Gagnoud, A.; Fautrelle, Y.; Ren, Z.; Li, X. Influence of a static magnetic field on the distribution of solute Cu and interdendritic constitutional undercooling in directionally solidified Al-4.5wt.%Cu alloy. *Mater. Lett.* **2019**, *248*, 73–77. [CrossRef]
103. Li, X.; Gagnoud, A.; Fautrelle, Y.; Ren, Z.; Moreau, R.; Zhang, Y.; Esling, C. Dendrite fragmentation and columnar-to-equiaxed transition during directional solidification at lower growth speed under a strong magnetic field. *Acta Mater.* **2012**, *60*, 3321–3332. [CrossRef]
104. Li, X.; Fautrelle, Y.; Ren, Z.; Zhang, Y.; Esling, C. Effect of a high magnetic field on the Al-Al_3Ni fiber eutectic during directional solidification. *Acta Mater.* **2010**, *58*, 2430–2441. [CrossRef]
105. Li, C.; Ren, Z.; Shen, Y.; Wang, Q.; Dai, Y.; Wang, H. Faceted growth of primary Al_2Cu crystals during directional solidification in high magnetic field. *J. Appl. Phys.* **2013**, *114*, 154903. [CrossRef]
106. He, S.; Shevchenko, N.; Eckert, S. In situ observation of directional solidification in Ga-In alloy under a transverse DC magnetic field. *IOP Conf. Ser. Mater. Sci. Eng.* **2020**, *861*, 012025. [CrossRef]
107. Koe, B.; Abraham, C.; Bailey, C.; Greening, B.; Small, M.; Connolley, T.; Mi, J. A novel electromagnetic apparatus for in-situ synchrotron X-ray imaging study of the separation of phases in metal solidification. *HardwareX* **2020**, *7*, e00104. [CrossRef] [PubMed]
108. Song, Z.; Magdysyuk, O.V.; Sparks, T.; Chiu, Y.-L.; Cai, B. Revealing growth mechanisms of faceted Al_2Cu intermetallic compounds via high-speed Synchrotron X-ray tomography. *Acta Mater.* **2022**, *231*, 117903. [CrossRef]
109. Kakeshita, T.; Saburi, T.; Shimizu, K. Effects of hydrostatic pressure and magnetic field on martensitic transformations. *Mater. Sci. Eng. A* **1999**, *273–275*, 21–39. [CrossRef]
110. Magomedov, M.N. On the magnetic-field-induced changes in the parameters of phase transitions. *Tech. Phys. Lett.* **2002**, *28*, 73–79. [CrossRef]
111. Aoki, Y.; Hayashi, S.; Komatsu, H. Liquidus- and eutectic-temperature measurements of Al-rich alloys containing Cu and Si in a magnetic field of 3.5 T. *J. Cryst. Growth* **1992**, *123*, 313–316. [CrossRef]
112. Long, Z.; Wang, J.; Fautrelle, Y.; Li, X. Repeated nucleation behaviors of pure bismuth under a high magnetic field. *J. Cryst. Growth* **2020**, *831*, 154746. [CrossRef]
113. Li, C.; Yang, H.; Ren, Z.; Ren, W.; Wu, Y. Application of differential thermal analysis to investigation of magnetic field effect on solidification of Al-Cu hypereutectic alloy. *J. Alloys Compd.* **2010**, *505*, 108–112. [CrossRef]
114. Li, C.; Guo, R.; Yuan, Z.; Xuan, W.; Ren, Z.; Zhong, Y.; Li, X.; Wang, H.; Wang, Q. Magnetic-field dependence of nucleation undercoolings in non-magnetic metallic melts. *Philos. Mag. Lett.* **2015**, *95*, 37–43. [CrossRef]
115. Guo, R.; Shuai, S.; Zhao, R.; Li, C.; Li, X.; Zhong, Y.; Wang, J.; Ren, Z. Enhanced Degradation in Grain Refinement of Inoculated 2024 Al Alloy in Steady Magnetic field. *Metall. Mater. Trans. A* **2020**, *51*, 4584–4591. [CrossRef]
116. Huang, C.; Shuai, S.; Li, C.; Wang, J.; Wang, J.; Shi, L.; Li, S.; Nan, R.; Ren, Z. Magnetic field-induced variation of solid/liquid interfacial energy of solid Al_2Cu and Al-Cu eutectic melt. *J. Alloys Compd.* **2023**, *941*, 168977. [CrossRef]
117. Wang, L.; Long, Z.; Hou, L.; Yan, S.; Sun, B.; Li, X. Effects of a high magnetic field on single-phase interface evolution, additional interfacial energy and nucleation undercooling in Al-based alloy. *J. Mater. Sci. Technol.* **2023**, *154*, 43–53. [CrossRef]

118. Liu, C.; Zhong, Y.; Shen, Z.; Zheng, T.; Dong, L.; Ren, W.; Lei, Z.; Ren, Z. Effect of an axial high static magnetic field on the crystal orientation and magnetic property of Fe-4.5wt.%Si alloy during bulk solidification. *Mater. Lett.* **2019**, *247*, 189–192. [CrossRef]
119. Morikawa, H.; Sassa, K.; Asai, S. Control of precipitating phase alignment and crystal orientation by imposition of a high magnetic field. *Mater. Trans. JIM* **1998**, *39*, 814–818. [CrossRef]
120. Dong, S.; Liu, T.; Dong, M.; Wang, S.; Wang, W.; Wang, K.; Wang, Q. Crystallographic orientation of primary and eutectic phases in a hypoeutectic Mn-Sb alloy induced by solidification in high magnetic fields. *J. Appl. Crystallogr.* **2019**, *52*, 945–950. [CrossRef]
121. Li, X.; Fautrelle, Y.; Moreau, R.; Ren, Z. EBSD study of the morphology and orientation of the primary and eutectic phases in Al-Cu alloys during solidification under a strong magnetic field. *J. Appl. Crystallogr.* **2016**, *49*, 139–148. [CrossRef]
122. Han, Y.; Ban, C.; Guo, S.; Liu, X.; Ba, Q.; Cui, J. Alignment behavior of primary Al3Fe phase in Al-Fe alloy under a high magnetic field. *Mater. Lett.* **2007**, *61*, 983–986. [CrossRef]
123. Wang, C.; Wang, Q.; Wang, Z.; Li, H.; Nakajima, K.; He, J. Phase alignment and crystal orientation of Al_3Ni in Al-Ni alloy by imposition of a uniform high magnetic field. *J. Cryst. Growth* **2008**, *310*, 1256–1263. [CrossRef]
124. Luo, D.; Guo, J.; Yan, Z.; Li, T. Effect of high magnetic fields on the solidification microstructure of an Al-Mn alloy. *Rare Met.* **2009**, *28*, 302–308. [CrossRef]
125. Mikelson, A.E.; Karklin, Y.K. Control of crystallization processes by means of magnetic fields. *J. Cryst. Growth* **1981**, *52*, 524–529. [CrossRef]
126. Sugiyama, T.; Tahashi, M.; Sassa, K.; Asai, S. The Control of Crystal Orientation in Non-magnetic Metals by Imposition of a High Magnetic Field. *ISIJ Int.* **2003**, *43*, 855–861. [CrossRef]
127. Lu, Y.; Dong, Y.; Guo, S.; Jiang, L.; Kang, H.; Wang, T.; Wen, B.; Wang, Z.; Jie, J.; Cao, Z.; et al. A Promising New Class of High-Temperature Alloys: Eutectic High-Entropy Alloys. *Sci. Rep.* **2014**, *4*, 6200. [CrossRef] [PubMed]
128. Shi, P.; Li, R.; Li, Y.; Wen, Y.; Zhong, Y.; Ren, W.; Shen, Z.; Zheng, T.; Peng, J.; Liang, X.; et al. Hierarchical crack buffering triples ductility in eutectic herringbone high-entropy alloys. *Science* **2021**, *373*, 912–918. [CrossRef] [PubMed]
129. Shi, P.; Ren, W.; Zheng, T.; Ren, Z.; Hou, X.; Peng, J.; Hu, P.; Gao, Y.; Zhong, Y.; Liaw, P.K. Enhanced strength-ductility synergy in ultrafine-grained eutectic high-entropy alloys by inheriting microstructural lamellae. *Nat. Commun.* **2019**, *10*, 489. [CrossRef]
130. Wang, J.; Long, Z.; Jiang, P.; Fautrelle, Y.; Li, X. Microstructure, Crystallographic Orientation and Mechanical Property in AlCoCrFeNi2.1 Eutectic High-Entropy Alloy Under Magnetic Field-Assisted Directional Solidification. *Metall. Mater. Trans. A* **2020**, *51*, 3504–3517. [CrossRef]
131. Deng, N.; Wang, J.; Wang, J.; He, Y.; Lan, Z.; Zhao, R.; Beaugon, E.; Li, J. Microstructure and properties of AlCoCrCuFeNi high-entropy alloy solidified under high magnetic field. *Mater. Lett.* **2021**, *285*, 129182. [CrossRef]
132. Frank-Rotsch, C.; Dropka, N.; Kießling, F.M.; Rudolph, P. Semiconductor Crystal Growth under the Influence of Magnetic Fields. *Cryst. Res. Technol.* **2019**, *55*, 1900115. [CrossRef]
133. Li, Q.; Xia, Z.; Guo, Y.; Shen, Z.; Zheng, T.; Ding, B.; Zhong, Y. Carbides Modification and Mechanical Properties Enhancement of Cr12MoV Die Steel by Magnetically Controlled Electroslag Remelting. *Metall. Mater. Trans. B* **2021**, *52*, 1495–1507. [CrossRef]